Water-Rock Interactions, Ore Deposits, and Environmental Geochemistry: A Tribute to David A. Crerar
© The Geochemical Society, Special Publication No. 7, 2002
Editors: Roland Hellmann and Scott A. Wood

Experimental pressure solution compaction of chalk in aqueous solutions

Part 1. Deformation behavior and chemistry

ROLAND HELLMANN[1*], PETER J.N. RENDERS[1**], JEAN-PIERRE GRATIER[1], AND ROBERT GUIGUET[1]

[1] Crustal Fluids and Dynamics Group, LGIT, CNRS UMR C5559, Observatoire de Grenoble,
Université J. Fourier, BP 53X, 38041 Grenoble Cedex 9, FRANCE
**present address: 211 Beekman St., Saratoga Springs, N.Y., 12866, U.S.A.

* corresponding author (hellmann@obs.ujf-grenoble.fr)

Abstract—To investigate pressure solution creep, chalk from the Paris basin (France) was deformed in a triaxial press with fluids. Experiments were conducted either under chemically closed (no fluid flow) or chemically open (fluid flow) conditions. In all experiments, the vertical stress (σ_1) and the lateral stress (σ_3) were independently controlled, with $4.0 < \sigma_1 \leq 8.0$ MPa and $\sigma_3 = 4.0$ MPa; the pore fluid pressure was ≤ 0.3 MPa. In each experiment, axial strain (ε) was recorded as a function of time; experiments ranged from 30 to almost 700 days.

The major goal of this investigation was to study the physico-chemical reactions that occur when chalk is deformed under different differential stresses, in the presence of various fluids, and at temperatures ranging up to 80 °C. The results show that chalk deformation is characterized by viscous behavior, based on plots of log strain rate ($\dot{\varepsilon}$) vs. log (σ_1) with slopes of 1-2. The chemical nature of the pore fluid also plays a critical role in determining deformation rates; the strain rates decreased in the following order: saline solution > water > propanol. Thus, strain rate correlates with calcite solubility. The dependence of $\dot{\varepsilon}$ on grain diameter could not be evaluated. The temperature dependence of strain rates was found to be very low, with an activation energy estimated to be ≈ 1-2 kJ mol^{-1}. When all rate-influencing parameters were kept constant, the material strain hardens, according to the relation $\dot{\varepsilon} \propto \varepsilon^{-2-5}$. The exact rate-limiting step (intergranular diffusion, dissolution, or precipitation) could not be determined based on the available data.

1. INTRODUCTION

1.1. Importance of Pressure Solution

In the crust, a very important percentage of material transfer occurs by way of water-rock interactions, which can be characterized in terms of both physical erosion processes and chemical weathering reactions. Chemical weathering reactions that occur at the surface and at shallow depths (≤ 1 km) occur predominantly by dissolution reactions, where dissolution takes place at essentially hydrostatically-stressed fluid/solid interfaces. This implies that dissolution reactions occur under isotropic conditions, and therefore, these reactions can be considered to be equally effective in all directions with respect to fluid attack of mineral grains comprising rocks.

Water-rock interactions within the crust, however, become increasingly anisotropic with increasing depth, this being a function of the divergence of the lithologic and hydrostatic gradients with depth. A commonly occurring and important water-rock interaction process at shallow to moderate depths is called pressure solution, or intergranular pressure solution (*ips*) creep. It occurs in geological environments in the upper crust that are characterized both by moderate levels of differential stress (i.e., at stress levels below those leading to brittle or plastic deformation) and the presence of fluids. Due to the fact that rocks at depth are exposed to differential stresses (i.e., vertical stress ≠ lateral stress ≠ pore fluid pressure), chemical instabilities develop on the scale of individual rock grains and the associated fluids in intergranular regions and pore spaces. As a consequence, there is a net transfer of material from regions of high stress along grain contacts to regions of lower stress in pore spaces, as schematically shown in Fig. 1.

The effective result of pressure solution is the deformation of individual mineral grains and precipitation of material in pore spaces, leading to a global compaction of the rock, and in general, a concomitant decrease in permeability. Pressure solution plays an important role with respect to chemical reactions, mass redistribution, and porosity changes associated with diagenesis of sediments and sedimentary rocks. In fact, pressure solution may be one of the primary processes responsible for the local production of dissolved material that precipitates as cements during diagenesis and burial cementation (e.g., Hudson, 1975; Wong and Oldershaw, 1981). Closely related to this is the evolution of permeability and porosity, as well as the channelization of fluids in sedimentary

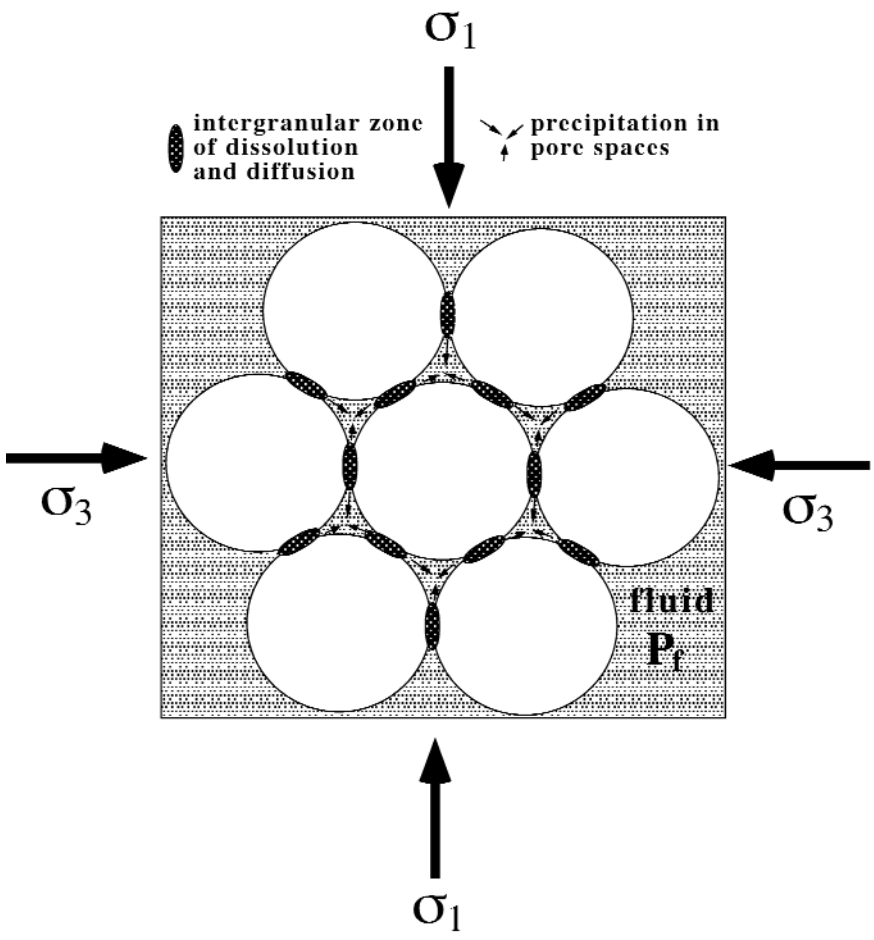

Fig. 1. Rock grains subject to a differential stress, where the vertical stress (σ_1) > lateral stress (σ_3); the interconnected pore spaces contain a fluid at pressure P_f, with $P_f < \sigma_1, \sigma_3$. Grain surfaces in contact with these pore fluids (free faces) are assumed to be in chemical equilibrium, such that no net dissolution occurs. Dissolution and diffusion occur at grain-to-grain boundaries subject to elevated stresses (dark stippled oval areas), precipitation occurs in pore spaces (advection of solutes is not considered). The net result is compaction of the grains and porosity reduction, coupled with a potential decrease in permeability, as well.

basins and other shallow geological environments (e.g., Ortoleva et al., 1987a, b).

Pressure solution creep is considered to be an important mechanism of rock deformation in the upper crust, along with mechanical compaction due to grain sliding, cataclasis (i.e., brittle failure of rocks due to crack propagation or frictional slip), and plastic deformation (i.e., a function of defect motion in crystals). What primarily differentiates pressure solution from these other deformation mechanisms is that it is a chemical process associated with intergranular dissolution and diffusion of material in a fluid phase. Pressure solution deformation is generally accepted to be limited to depths less than 15-20 km, with pressure and temperature (P,T) conditions ranging up to greenschist facies (Tada and Siever, 1989). At these P,T conditions, pressure solution and cataclastic deformation may act in a coupled fashion, such that the crust behaves in both a viscous and brittle manner (see Gratier and Gamond, 1990; Gratier et al., 1999). At higher P,T conditions, plastic deformation becomes the dominant creep mechanism (see overview in Chen and Molnar, 1983; and references therein).

There are at least 11 processes that can lead to deformation and compaction of granular minerals, one of which is pressure solution (described in Fig. 15.1, Evans et al., 1999). Some of the key factors in determining the importance of each type of deformation process are temperature, pressure, applied stress, and chemical fugacities of the phases. With this in mind, it

is important to note that both in nature and in the laboratory, deformation and compaction of granular aggregates probably are a function of many simultaneously operating processes, with each process having a different degree of overall importance. Even a single type of process, such as pressure solution, may depend on several distinct mechanisms, as described further on.

Over the past two to three decades, theoretists have developed and refined models treating non-hydrostatically-stressed solids and pressure solution reactions (e.g., Rutter, 1976; Lehner and Bataille, 1985; Paterson, 1973, 1995; Tada et al., 1987; Bayly, 1987, Dewers and Ortoleva, 1989; Gratz, 1991; Lehner, 1995; Renard et al., 1999). Numerical experiments serve as a basis for modeling a variety of geological phenomena at diverse scales, ranging from compaction of sedimentary basins (e.g., Lemée and Guéguen, 1996; Schneider et al., 1996), the segregation of minerals in metamorphic rocks (e.g., Robin, 1979; Dewers and Ortoleva, 1990b), densification and compaction of aggregates and unconsolidated materials in the laboratory (e.g., Elias and Hajash, 1992; Spiers and Brzesowsky, 1993), to the evolution of pore space geometries under differential stress (e.g., Reuschlé et al., 1988; Heidug and Leroy, 1994; Leroy and Heidug, 1994).

It has long been recognized that fluids play an active role in determining the dynamics and strength of faults, mainly by affecting physical mechanisms (e.g., friction, fluid pressure). It has become increasingly evident, however, that the role of fluids in faults is not just limited to mechanical effects, but that the chemical role of fluids is also of great importance. The chemistry of fluids and chemical water-rock interactions may play a role in determining, for example, fault creep behavior, brittle fracture behavior, constitutive response, frictional stability, and long-term fault strength (Hickman et al, 1995; and references therein). More specifically, pressure solution reactions have been postulated to play an important role in the rheology and strength of faults within the framework of the aseismic/seismic cycle of faults (e.g., Rutter and Mainprice, 1979, Angevine et al., 1982, Sleep and Blanpied, 1992; Gratier et al., 1994; Hickman et al., 1995; and references therein). Studies of fault zones occurring in limestones and chalks have revealed that compaction, attributed to pressure solution and cementation, increases to a significant extent close to fault planes (e.g., Carrio-Schaffhauser and Gaviglio, 1990; Gaviglio et al., 1993, 1997).

Experimental approaches to pressure solution have generally been based on the deformation of unconsolidated materials, such as quartz and feldspathic sand (de Boer et al., 1977; Gratier and Guiguet, 1986; Schutjens, 1991; Hajash and Bloom, 1991; Elias and Hajash, 1992; Dewers and Hajash, 1995), aggregates (salt: Raj, 1982; Urai et al., 1986; Spiers et al., 1990; Spiers and Brzesowsky, 1993; Hellmann et al., 1998; gypsum: de Meer and Spiers, 1995, 1997; quartz: Cox and Patterson, 1991), or porous, natural rocks (chalk: Hellmann et al., 1996; quartzite: e.g., den Brok and Spiers, 1991; den Brok, 1996). Another approach that is occasionally used is the indenter technique (Tada and Siever, 1986; Tada et al., 1987; Gratier, 1993; Gratier et al., 1999). Other, more uncommon approaches also have been used to study pressure solution; for example, a study by Hickman and Evans (1995) where deformation of halite-silica lenses was monitored by reflected light interferometry and transmitted light photomicrography.

Despite that many experimental approaches have been used to study pressure solution, there remains a fundamental discrepancy between natural rates of pressure solution, which are extremely slow, and those measured in the laboratory, which by practical necessity, are much faster (de Boer, 1977). Elevated rates of pressure solution deformation are generally realized in the laboratory by applying much higher loading rates than occur naturally. As an example, typical loading rates associated with North Sea oil reservoirs are on the order of 10^{-8} MPa s^{-1}, whereas laboratory loading rates are usually on the order of 10^{-2} -10^{-4} MPa s^{-1} (Monjoie et al., 1991). In addition to the use of high loading rates, experimental studies also rely on elevated temperatures and/or chemically aggressive fluids to accelerate the rates of deformation in the laboratory. This approach of accelerated deformation carries with it the potential danger that measured deformation rates result from mechanisms or reactions that may be different from those occurring naturally.

1.2. Chalk Deformation: Mechanical and Chemical Processes

The present study is based on the experimental deformation of natural chalk in the presence of aqueous and non-aqueous fluids. Chalk is a material which is of broad interest in the fields of geology, petroleum and civil engineering, and radwaste storage. Especially because of its importance with respect to oil reserves (e.g., North Sea), many studies over the past few decades have been dedicated to understanding the mechanical properties and deformation behavior of chalk, both dry and in the presence of fluids (e.g., Botter, 1985; Da Silva et al., 1985; Jones and Leddra, 1989; Monjoie et al., 1990; Shao et al., 1994; Piau and Maury, 1995; Schroeder and Shao, 1996; Homand et al., 1998; Risnes and Flaageng, 1999; see also references in GBMR, 1995).

Taking a recent study by Homand et al. (1998) as a representative example, the deformation of chalk in the presence of fluids is modeled using an elasto-plastic constitutive law, where the total strain tensor is partitioned into elastic ($d\varepsilon_{ij}^{e}$), plastic collapse ($d\varepsilon_{ij}^{c}$), and plastic deviatoric ($d\varepsilon_{ij}^{d}$) components, such that: $d\varepsilon_{ij} = d\varepsilon_{ij}^{e} + d\varepsilon_{ij}^{c} + d\varepsilon_{ij}^{d}$. The elastic strain is more correctly called pseudo-elastic, since not all of the strain is recoverable, and in addition, the strain is time-dependent. The second strain component is due to pore collapse, which is induced by the physico-chemical breaking of grain-to-grain bonds or disruption of attractive forces, this permitting grain sliding to take place (Monjoie et al., 1991). Pore collapse leads to a porosity decrease on the order of just ≈ 1% (Schroeder, 1995). The effective axial stress threshold that leads to pore collapse (also called the yield stress) strongly depends on external parameters, such as effective pressure, deformation rate, and temperature, as well as on internal parameters, such as the porosity, the amount and type of impurities (e.g., silica content, Da Silva et al., 1985), and especially on the nature of the pore fluids (e.g., Schroeder, 1995; Schroeder and Shao, 1996). The yield strength can be as low as 5-7 MPa for a high porosity (>45%), water-saturated chalk (Schroeder and Shao, 1996). The plastic deviatoric strain component is assumed to be due to matrix distortion due to shearing. For strains greater than 10%, a 2nd plastic deformation occurs with a stronger degree of hardening than in the first stage of plastic deviatoric deformation (Monjoie et al., 1991). Note that the use above of the term plastic deformation with respect to mechanical deformation does not imply a specific mechanism (i.e., dislocation flow).

The main reason for undertaking the present study was to examine the wet deformation of chalk at modest stress levels, where deformation can be primarily attributed to pressure solution. Until now, the deformation of chalk has almost exclusively been investigated and interpreted from the standpoint of mechanical deformation processes, whereas pressure solution has received at most only scant attention as a possible deformation mechanism. The stress conditions associated with deformation in the present study overlap with the lower effective stress fields in most of the chalk deformation studies mentioned immediately above. As will be discussed further on in more detail, much of the deformation behavior (at moderate stress levels) that has been traditionally attributed to mechanical processes may actually be more accurately understood in terms of pressure solution, where chemical reactions at stressed grain-to-grain boundaries cause deformation.

In this study, natural chalk samples were deformed in the presence of fluids over long time periods, up to almost 700 days. The axial compaction of the samples was recorded as a function of time. The primary aim of these experiments was to study the physico-chemical reactions that occur when chalk is deformed under different differential stresses in the presence of various types of fluids at temperatures ranging from 25 to 80 °C. This enabled us to investigate the various deformation rate-influencing parameters within the framework of published constitutive pressure solution relations, with the ultimate goal of better understanding the mechanisms of pressure solution. This constitutes Part 1 of this communication.

The pressure solution deformation of chalk was also investigated by examining the redistribution of mass within the matrix, as evidenced by measured changes in porosity and density before and post-deformation. This investigation is primarily based on the results from two experiments (L9-11 and L16), and is detailed in Part 2.

2. MECHANISMS AND MODELS OF PRESSURE SOLUTION: A BRIEF REVIEW

2.1. Thermodynamics of Pressure Solution

Among the first attempts to describe the thermodynamics of solids in contact with fluids at varying pressures were pioneering studies by Sorby (1863) and Gibbs (1878). More than a century later, uncertainties still remain in our understanding of non-hydrostatically stressed solids and the mechanisms of pressure solution (Evans and Kohlstedt, 1995). Even though a detailed analysis of the thermodynamic and kinetic driving forces associated with pressure solution is beyond the scope of this article (see e.g., Paterson, 1973; Bayly, 1985, 1987; Lehner and Bataille, 1985; Lehner, 1990 for detailed discussions; see also transport models in Table 4, Evans and Kohlstedt, 1995), a short review is given below, with the aim of helping readers unfamiliar with intergranular pressure solution creep understand the analysis of the chalk deformation data that is given later on.

As mentioned earlier in the *Introduction*, rocks at depth in the presence of fluids develop chemical instabilities on the scale of individual rock grains. This gives rise to differences in the chemical potentials of the individual solid constituents (e.g., μ_{Si}) along various grain surfaces. The following example (see Fig. 2), based on two interfaces of the same grain that are subject to different stresses, is used to illustrate how these differences in chemical potential arise. Both equilibrium and non-equilibrium thermodynamic ap-

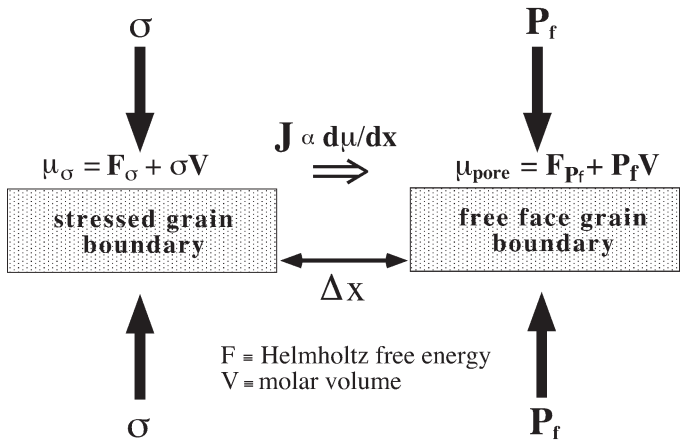

Fig. 2. The main thermodynamic driving force of pressure solution is the difference in chemical potentials ($\Delta\mu = \mu_\sigma - \mu_{pore}$) between a fluid-solid interface, subject to normal stress σ, and a pore fluid-solid interface, subject to hydrostatic stress P_f (P_f = pore pressure). The chemical potentials of the solid interfaces and the respective fluids in contact with them are assumed to be equal, based on a 'local equilibrium' approximation. The flux of dissolved material diffusing between the stressed interface and the pore fluid interface is a function of $\Delta\mu$ and the intergranular diffusion distance Δx.

proaches (e.g., Kamb, 1959, 1961; Paterson, 1973; Lehner and Bataille, 1985) lead to the following expressions (see original derivation by Gibbs, 1878) for the respective chemical potentials of an interface subject to a compressive normal stress σ and an interface subject to a hydrostatic stress P_f:

$$\mu_\sigma = F_\sigma + \sigma V_\sigma \quad ; \qquad \mu_{pore} = F_{Pf} + P_f V_{Pf} \quad (1a)$$

In the above equations F is the Helmholtz free energy of the solid (i.e., energy associated with stored elastic and strain energies, which are a function of applied stresses), and V_σ and V_{Pf} are the molar volumes of the σ-stressed and pore fluid pressure-stressed solids, respectively (the small difference in these terms is usually neglected). Equation 1a neglects radius of curvature effects, which are assumed in this case not to be important. The differences in chemical potentials of these two interfaces are also shown graphically in Fig. 2. In Eqn. 1a, $\mu_\sigma > \mu_{pore}$, due to the fact that $F_\sigma > F_{Pf}$ and $\sigma V_\sigma > P_f V_{Pf}$. Note that an assumed condition of "local equilibrium" between a stressed interface and the fluid in contact with it (Kamb, 1961; Paterson, 1973) allows the chemical potential of any given component in the solid to be equated to its chemical potential in the fluid (e.g., $\mu_{Si\ solid\ \sigma} = \mu_{Si\ aq\ \sigma}$).This approximation, however, should not be construed to mean that a *true* chemical equilibrium exists at the solid/fluid phase interface (see Lehner, 1995).

The difference in chemical potentials:

$$\Delta\mu = (\sigma - P_f)V + (F_\sigma - F_{P_f}) \quad (1b)$$

is the essential thermodynamic driving force for the overall process of pressure solution which leads to the enhanced solubility of stressed interfaces and the diffusional transfer of dissolved material to regions of lower stress, such as pore spaces (see Figs. 1, 2).

Since $\Delta\mu$ is the essential energy driving pressure solution, then according to Eqn. 1b, the higher the normal compressive stress is, the greater $\Delta\mu$ will be, due to increases in the terms $(\sigma - P_f)V$ and $(F_\sigma - F_{P_f})$. Thus, referring to Fig. 1, the grain-to-grain contacts perpendicular to σ_1 are theoretically predicted to converge at a faster rate than the contacts perpendicular to σ_3 (i.e., pressure solution deformation will be fastest parallel to σ_1). In general, the overall difference in the chemical potentials is due primarily to $\sigma V > P_f V$, while the difference in the Helmholtz energy terms is significantly less (Paterson, 1973). However, some pressure solution models are based explicitly only on differences in the Helmholtz energy terms. Given that pressure solution is based on the serial processes of dissolution, diffusion, and precipitation, all three processes will consume the total available free energy ($\Delta\mu$). The partitioning of $\Delta\mu$ among the three processes is thought to be a function of which process is rate-determining; the slowest (rate-limiting) step will consume the vast majority of this energy (see Lehner, 1995).

From the above analysis of pressure solution, one could be led to believe that only the thermodynamic

force $\Delta\mu$ will determine the rate of grain-to-grain convergence. However, observations based on nature and laboratory results clearly show that for the same differential stress ($\sigma - P_f$), different materials deform at different rates. This is because the actual rate of grain-to-grain convergence is a function of a force-flux relationship, and not just the force. Thus, considering the dissolution process at a stressed interface, a simple linear force-flux relation of the following form can be postulated (adapted from Lehner, 1995):

$$\dot{m} \propto K\,[\mu_n^s(r) - \mu(r)] \tag{1c}$$

where $\dot{m}$ is the flux, K is a rate constant, and the quantity in brackets is the chemical potential driving force (with $\mu_n^s(r)$ equal to the normal component of the solid phase chemical potential and $\mu(r)$ equal to the fluid phase potential in the grain boundary region). A similar relation can be expressed for precipitation, with the appropriate changes made to the chemical potential driving force. The diffusion process can also be represented in terms of a force-flux relationship, based on Fick's Law. Therefore, for the diffusion flux one can write (adapted from Lehner, 1995):

$$\dot{m} \propto C_0\, D^{gb}\delta / a^2\,[\tilde{\mu} - \mu(a)] \tag{1d}$$

where C_0 is a reference concentration equal to the solubility of the solid in the pore fluid, D^{gb} is the effective grain boundary diffusivity, δ is the mean grain boundary thickness, a is the grain boundary radius, and $[\tilde{\mu} - \mu(a)]$ is the average chemical potential driving force. Equations 1c and 1d form the basis of most constitutive relations for pressure solution deformation. Often just one of these relations is given preference based on an *a priori* choice as to which process is thought to be rate-limiting.

Thus, Eqns. 1c and 1d are the key to understanding why different materials deform at different rates, when all other rate-determining parameters are equal. Taking halite and quartz for example, one can predict that halite grain-to-grain convergence will be faster than quartz convergence, based on the fact that $K_{diss}^{halite} >> K_{diss}^{qtz}$, or $C_0^{halite} >> C_0^{qtz}$. These kinetic and solubility factors far outweigh any potential differences in the constitutive properties of the solid related to the Helmholtz free energy (Eqns. 1a and b).

2.2. Pressure Solution Models

The first model, often called free-face pressure solution, is based on the premise that grain-to-grain contacts are dry, and that dissolution only occurs at grain surfaces in contact with pore fluids (these surfaces are called 'free faces'). Dissolution along free faces at the perimeters of the grain contacts, which are accelerated by elevated surface strain and plastic energies (e.g., Dewers and Ortoleva, 1989), results in undercutting and a reduction in the intergranular contact area, this eventually leading to deformation of intergranular boundaries, either by plastic dislocation flow (e.g., Pharr and Ashby, 1983; Tada and Siever, 1986; Tada et al. 1987) or by brittle failure (Bathurst, 1958).

The second and third models are both based on grain-to-grain contacts that contain a trapped fluid which cannot be squeezed out by the normal stresses imposed on the grains. In addition, both of these models are based on 3 material transfer processes occurring in series:dissolution at stressed intergranular regions, diffusion of dissolved material along stressed grain-to-grain boundaries, and precipitation in pore spaces. It is primarily the physical nature of the intergranular regions that differentiates these two models, which often are referred to as the water-film diffusion and island-channel models, respectively.

The water-film diffusion model is based on the presence of a continuous thin film of fluid at grain-to-grain contacts that is able to support a shear stress (e.g., Weyl, 1959; Elliot, 1973; Rutter, 1976, 1983; Hickman and Evans, 1995; Renard and Ortoleva, 1997). This thin fluid film (≈ 1-30 nm) is postulated to have very special properties with respect to a bulk fluid, both in terms of surface forces and the structured nature of the fluid molecules (see discussion in Heidug, 1995; and references therein), as well as with respect to the thermodynamic and transport properties (e.g., Weyl, 1959; Robin, 1978; Rutter, 1976, 1983; Tada et al., 1987). Experimental evidence for such thin films is quite circumstantial at present, however.

As the name suggests, the island-channel model posits an intergranular region consisting of solid-solid contacts at islands (with μm to atomic scale roughness) that support the imposed normal stresses; these islands are surrounded by a network of interconnected channels containing fluid (e.g., Raj, 1982; Spiers et al., 1990; Cox and Patterson, 1991; Schutjens and Spiers, 1999). If the interconnected channels are directly connected to the pore fluid, then the fluid pressures should be equal. This is supported by intergranular diffusion rates that are estimated to be equivalent to those in bulk fluids or pore spaces (e.g., Raj and Chyung, 1981; Spiers et al., 1990; Lehner, 1990). Given that the normal compressive stresses acting along wetted intergranular surfaces are considered to be equal to the fluid pressure in adjacent pore spaces, the gradient in chemical potentials between the wetted intergranular regions and the pore spaces should logically *not* be due to $(\sigma - P_f)V$, but rather to differences in $(F_\sigma - F_{P_f})$, the Helmholtz energy (refer to Eqn. 1b). Stress concentrations at the islands within the intergranular zone, due in part to undercutting,

also lead to deformation, either through brittle failure or plastic dislocation flow. Nonetheless, most studies that model pressure solution using the island-channel model still consider that the primary driving force is $\Delta\mu \propto (\sigma - P_f)V$ (e.g., Raj and Chyung, 1981; Spiers et al., 1990). This contradiction can only be alleviated by assuming that the fluid pressure in the intergranular regions is higher than that in pore spaces and that the intergranular fluid is not directly connected to the pore fluid. Despite similarities with the free-face model, the island-channel model stresses that preferential dissolution and the outward diffusion of dissolved material occur exclusively within the intergranular zone, and not in pore spaces.

The dynamic stability of interface roughness is a subject of debate. There is evidence that surface roughness between wetted grains decreases over time, but that a certain degree of micro-roughness prevails, due to the effects of heterogeneous dissolution (i.e., influence of defects, impurities, etc.) (Spiers and Schutjens, 1990; Lehner, 1990). As an example, the time evolution of a halite-halite interface has been observed to start with μm-scale roughness and progress to <500 nm roughness by Schutjens and Spiers (1999). Based on entropy considerations, Raj (1982) postulated that islands (surface roughness) are thermodynamically stable.

It should be noted that the three pressure solution models presented above are not necessarily mutually exclusive. As an example, Gratz (1991) proposed a hybrid water-film/island-channel model, where load-supporting islands are capped by a thin fluid film. In addition, in laboratory studies (e.g., Gratier, 1993) and in natural cases (e.g., Engelder, 1982), both intergranular and free-face pressure solution mechanisms have been inferred to be operative. In addition to the above factors, studies have shown that pressure solution deformation rates are usually significantly faster when solids of different composition are in contact, in comparison to solids having the same composition (e.g., Dewers and Ortoleva, 1991; Hickman and Evans, 1995). This has important ramifications with respect to rates of pressure solution in nature where, for example, it is often observed that clays occupy grain-to-grain contacts in sandstones.

Both Figs. 1 and 2 show the three principal material transfer processes that operate in series during pressure solution: dissolution, diffusion, and precipitation. It is assumed that advective transport of material between pore spaces does not occur. Since in a serial process the slowest step is rate-controlling, one of the 3 material transfer steps will determine the overall rate of pressure solution deformation of an aggregate. In free-face pressure solution, the interfacial kinetics (i.e., dissolution or precipitation in pore spaces) or the constitutive properties of the solid are rate-limiting (Tada et al., 1987). On the other hand, with respect to intergranular pressure solution (water-film and island-channel models), most studies in the literature postulate diffusion as the rate-limiting step (e.g., Weyl, 1959; Elliot, 1973; Rutter, 1976; Gratier and Guiguet, 1986; Hickman and Evans, 1995). However, in the case of sparingly soluble minerals (e.g. quartz, gypsum), surface processes, such as dissolution or precipitation, may instead be the rate-limiting process (e.g., Raj and Chyung, 1981; Mullis, 1991, 1993; de Meer and Spiers, 1995).

The rate-limiting step in pressure solution is either assumed *a priori* in a model (e.g., NaCl, Spiers et al., 1990), or alternatively, no *a priori* choice of rate-limiting process is imposed (e.g., Merino et al., 1983; Lehner, 1995). The criterion of rate control (i.e., the rate-limiting step), as well as the mechanism of deformation, may also change during deformation, depending on the exact conditions and rates of deformation, burial depth, grain diameters, and the chemical and physical characteristics of the fluids and solids (e.g., Lehner and Bataille, 1985; Tada et al. 1987; Spiers and Brzesowsky, 1993; Mullis, 1993; Renard et al., 1999).

The transfer of material from intergranular regions subject to elevated stress to pore spaces occurs by a grain boundary diffusional process, within a fluid phase (see dark gray oval zones in Fig. 1). Fick's first law can be used as an approximation to link the diffusive flux (J) from stressed intergranular regions to pore spaces as a function of the difference in chemical potentials in the fluid and the distance of diffusion (Δx) separating both regions: $J \propto \partial\mu/\partial x$. This simple diffusional flux relationship (see Fig. 2) is an integral part of most intergranular pressure models. The diffusional distance (Δx), which is often taken to be equal to the radius of grains, is not always easily constrained, however. One reason for this is experimental evidence for stress-induced micro-cracking on intergranular surfaces (e.g., Gratz, 1991; den Brok, 1998; Gratier et al., 1999). Micro-cracking may considerably diminish the distance of diffusion within the hypothesized thin fluid film. This phenomenon can also be considered to be a mechanism of strain.

3. EXPERIMENTAL MATERIALS AND PROCEDURES

3.1. Characteristics of the Chalk

The chalk used in this study was quarried from the Guerville formation (Carrière de Mantes, Guerville, France), a Campanian age chalk that crops out in the Mantes region within the Paris basin (for additional

details, see Megnien, 1980; and references therein). There was no visible stratigraphic layering within the 1/3 m^3 block from which the cores were extracted. Examination by optical microscopy and SEM reveals that the chalk is composed largely of coccolith skeletal debris and other shell fragments (see SEM image, Fig. 3a). The SEM image reveals numerous voids with diameters ranging from ≈1 to several μm. The magnification of the images was not sufficient to characterize the nature of the intergranular cement. X-ray diffraction results of 4 post-run samples taken from the same core (L16) show that the chalk is composed essentially of calcium carbonate: 3 samples show ≈100% calcite, whereas one sample shows the presence of a minor amount of dolomite (≈1%). The occurrence of dolomite may be related to Mg-rich fluids injected during the experiment. The representative surface area of the undeformed chalk, as measured by the BET method, is ≈ 1.4 m^2 g^{-1} (±15%).

The chalk is heterogeneous (visible even to the naked eye), and contains mm- to cm-sized chert fragments dispersed randomly throughout the chalk. Apparently non-oriented thin calcite veins cross-cut the sample over a cm-scale interval. These veins are composed of the same material as the chalk matrix (as confirmed by SEM/EDX analyses), but have more calcite cement, and are more compact and less porous than the matrix. Figure 3b is an SEM image of a typical vein cross cutting the chalk matrix; x-ray computerized tomography images in Fig. 15 (Part 2) show a macroscopic view of the vein network.

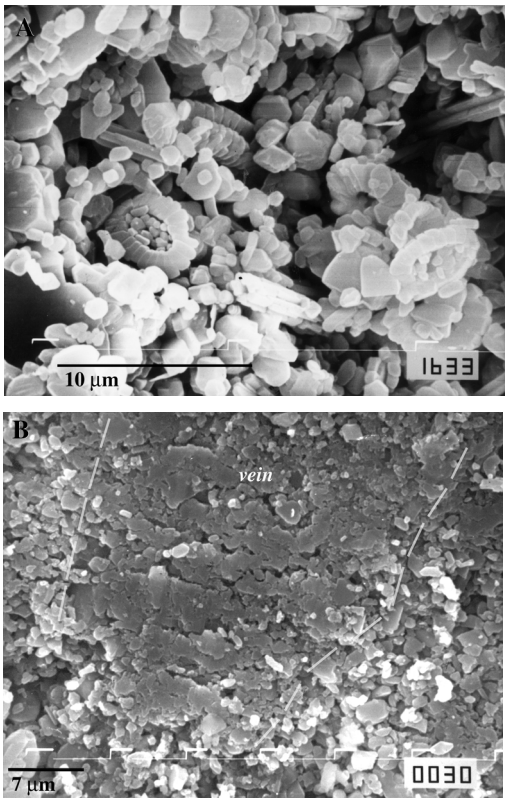

Fig. 3. SEM images of Guerville chalk used in study. (A) The chalk is composed primarily of coccolith skeletal debris and other shell fragments; note the high porosity inherent to this chalk. (B) Vein crosscutting the matrix; the porosity is considerably diminished in comparison to surrounding matrix.

3.2. Experimental Apparatus

Two core sizes were used for the deformation experiments: $\phi = 25$ mm, $l = 50$ mm and $\phi = 100$ mm, $l = 200$ mm. Figure 4 shows a schematic design of the triaxial deformation apparatus used in the large core experiments; the apparatus used for short cores is very similar. The vertical stress (σ_1) is imposed by gas pressure on a piston in contact with the core; the lateral stress (σ_3) is imposed directly by gas pressure acting on the entire vertical surface of the sheathed core. Note that the imposed vertical and lateral stresses are independent of each other. The indicated values of σ_1 have not been corrected for the effect of o-ring friction, as it is estimated to be ≈ 0.035 MPa.

A pump (HPLC or syringe design) serves to move fluids from bottom to top through the sample at a precise and constant rate. Injection rates (ν) were variable, but in general, they did not exceed 0.1- 0.2 ml min^{-1}; the measured inlet pressures were in general ≤ 0.3 MPa. Based on the aforementioned flow rates, the volumetric flow rates per unit area of connected pore space were 0.0032 - 0.0064 cm min^{-1} (i.e., effective Darcy velocities based on large core dimensions, and an average chalk porosity of 40%). As an example, a Darcy velocity of 0.0032 cm min^{-1} corresponds to a residence time of 6250 mins (104 hours) for fluids traversing the large cores. The fluid outflow is at ambient pressure; however, if a higher fluid pressure (P_f) is desired, the outflow tube is easily connected to a backpressure regulator which controls the fluid pressure. The top and bottom faces of the chalk cylinder are fitted with stainless steel cap plates incorporating a rectilinear grid of holes (mm-spacing between holes) to optimize the homogeneous infiltration of fluid into the sample. The entire pressure vessel, which incorporates 4 horizontal thermocouple temperature sensors, is heated by an external furnace (thermal stability ± 1 °C).

The vertical displacement of the piston is measured continuously using a mechanical micrometer with a resolution of 0.0002 mm. Radial strain could not be

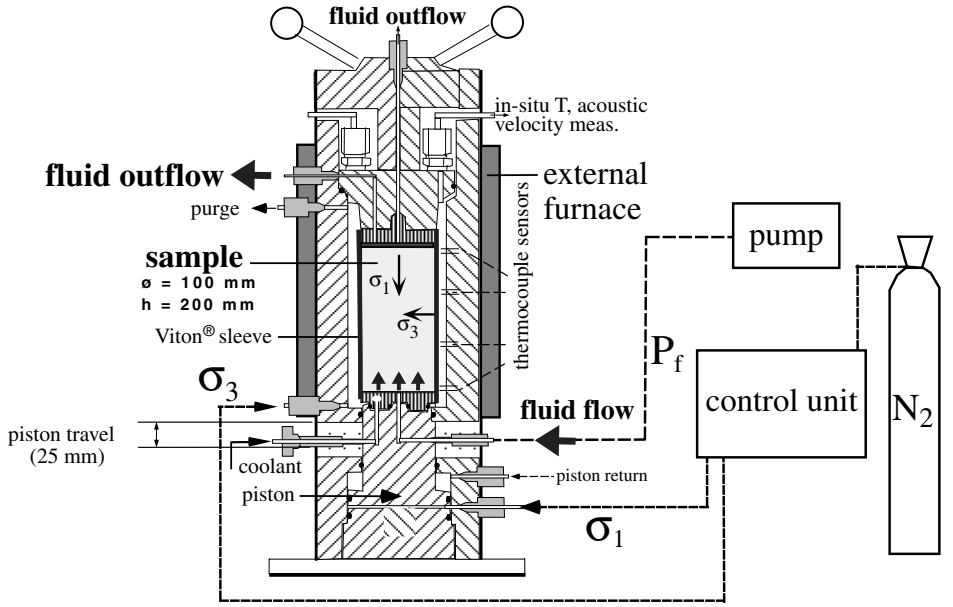

Fig. 4. Triaxial flow apparatus used in deformation experiments of large samples (200 mm length). The vertical and lateral stresses are independently controlled. Fluids are injected into the sample with a syringe or HPLC pump, fluid flow is from bottom to top. The fluid pressure can be controlled by connecting the outflow tubing to a back pressure regulator.

measured continuously during the experiment, but measurements with calipers at the end of experiments did not indicate any measurable radial strain. Measurement of the vertical displacement allows for determination of the axial strain (ε) at any specified time using the relation:

$$\varepsilon = \frac{l_0 - l}{l_0} \tag{2}$$

where l_0 is the original length of the sample and l is the length at a specified time. The vertical strain rate ($\dot{\varepsilon}$) at any specified time is equal to the time derivative of ε, normalized to the instantaneous length of the sample:

$$\dot{\varepsilon} = \frac{\partial l / \partial t}{l} \tag{3}$$

3.3 Experimental Procedures

Because the chalk is very fragile, it was not possible to core a single 200-mm long cylinder; instead, two smaller cores, approximately the same length, were placed end-to-end. The top and bottom faces of each core were cut and sanded perpendicular to the core axis. Before the cores were deformed, they were dried in an oven at ≈70-110 °C over periods ranging from several hours up to 2 days. This drying step greatly decreased the probability of core collapse during pressure loading. Before insertion into the deformation apparatus, the cylindrical body of chalk (composed of 2 cores) was sheathed with either a rubber or a Viton® sleeve (rubber used for T < 50 °C). This sleeve serves a double purpose: first, it provides an impermeable surface for transmitting the lateral stress to the sample; second, it prevents the escape of fluids from within the chalk core via the cylindrical walls of the core.

Initial pressure loading of the sample was performed in the absence of fluids at room temperature over the course of approximately 1 day. Loading was nominally non-hydrostatic ($\sigma_1 \geq \sigma_3$), with loading rates less than 0.1 MPa min^{-1}. Once the desired value of σ_3 was reached, the axial stress σ_1 was slowly increased to the final value, such that $\sigma_1 > \sigma_3$. After stabilization of the samples ($\dot{\varepsilon} \approx 0$) during the initial phase of dry deformation (over periods of up to 10 days), pressure solution deformation was initiated by the injection and infiltration of fluids into the samples. Aqueous fluids were degassed by boiling ≈ 1

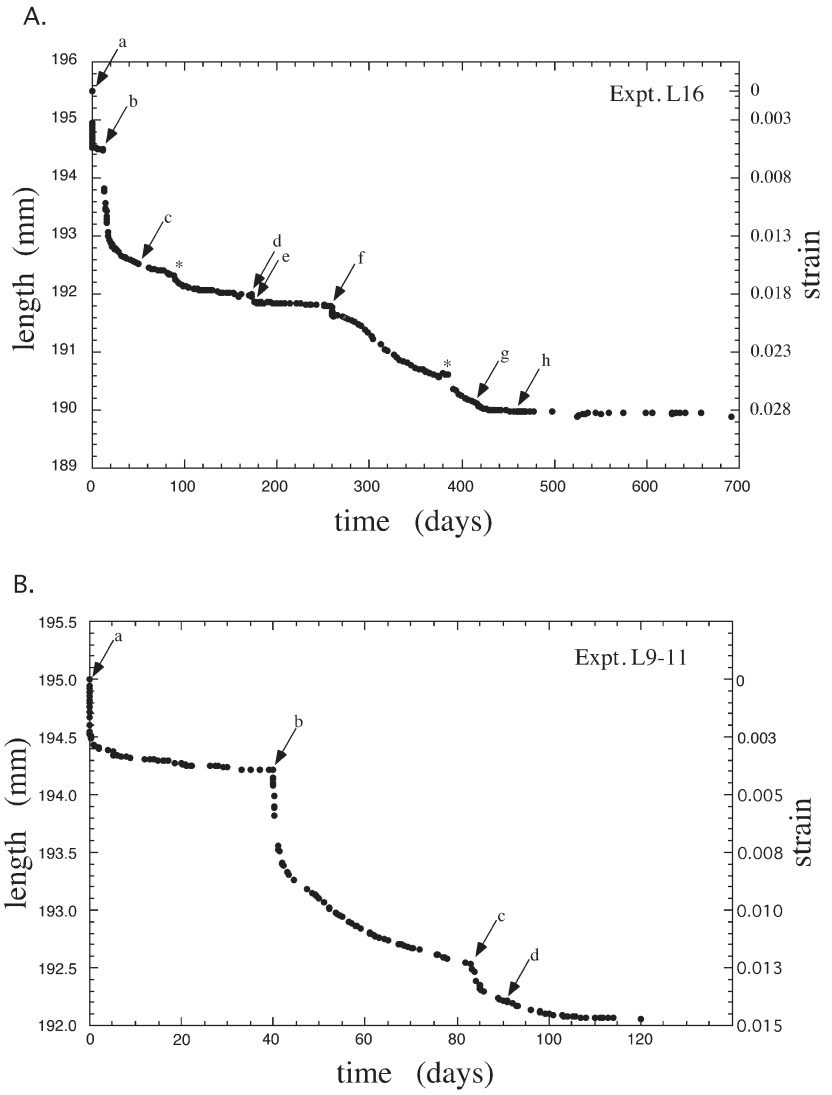

Fig. 5. Deformation curves for experiments L16 and L9-11 (note that strain (ε) increases in negative direction along ordinate axis). Changes in various strain rate-influencing parameters during the course of each experiment served to perturb local "steady-state" deformation behavior. (A) L16 parameter changes a: start of dry deformation, $\sigma_1 = 6.0$, $\sigma_3 = 4.0$ MPa, 25 °C b: injection H_2O, $v = 0.5 \rightarrow 0.1$ ml min^{-1}, T = 25 → 50 °C c: $v = 0$ over t = 50-172 days; *instability, gas bottle change d: injection saline solution over t = 179-189 days, v = variable e: $v = 0$ over t = 189-259 days f: T = 50 → 77 °C, $v = 0$ over t = 259-417 days; * instability, gas bottle change, $\sigma_1 = 7.0$, $\sigma_3 = 4.0$ MPa g: $v = 0.1$ ml min^{-1} over t = 417-461 days h: injection propanol, $v = 0.1 \rightarrow 0$ ml min^{-1}. (B) L9-11 parameter changes a: dry deformation: 0 - 0.08 days, followed by start of fluid-assisted deformation, injection H_2O, $v = 0.5 \rightarrow 0.2$ ml min^{-1}, $\sigma_1 = 4.9$, $\sigma_3 = 4.0$ MPa b: $\sigma_1 = 7.0$, $\sigma_3 = 4.0$ MPa, $v = 0.2 \rightarrow 0.1$ ml min^{-1} c: T = 25 → 50 °C d: injection of saline solution, $v = 0.1$ ml min^{-1}.

hour prior to injection into the sample; non-aqueous fluids (propanol) were not degassed and were assumed to be in equilibrium with $P_{CO_2 atm}$. Fluids were periodically sampled at the exit and analyzed for Ca and Mg by standard analytical techniques.

Experimental run times ranged from 30 to almost 700 days. The general experimental procedure consisted of allowing the system to attain a "steady-state" rate of deformation, over periods up to several weeks. Deliberate changes in any one of the defor-

mation rate-influencing parameters (σ_1, temperature, chemistry of input solution, injection rate, fluid pressure) served to perturb the steady-state behavior of the system, producing in most cases very abrupt changes in the deformation rate. These abrupt changes gave way to progressive stabilization and the establishment of new steady-state rates of deformation. Thus, the overall deformation behavior of samples can be described by a series of transitions from one local "steady state" to another, separated by abrupt changes in the deformation rate (see Figs. 5a, b). The exact meaning of "steady-state" deformation behavior refers to instantaneous deformation rates that are very slowly varying- this is discussed further on in more detail.

3.4. Experimental Conditions

In total, 5 experiments were run with small samples, 4 with large samples. Two experiments, L16 and L9-11, are described in detail below. The post-deformation cores of these two experiments were also analyzed in detail in terms of their porosity and density by various analytical techniques, as reported in Part 2.

Experiment L16 was run with the following applied stresses: σ_3 = 4.0±0.2 MPa, σ_1 = 6.0±0.2 MPa initially; towards the end of the experiment, σ_1 was increased to 7.0±0.2 MPa. The instabilities associated with σ_1 and σ_3 reflect the effects of slow pressure changes (i.e., non-optimal performance of pressure regulation system), as well as more sudden pressure fluctuations resulting from the occasional exchange of gas bottles that were used as the pressure medium. Four experimental parameters that influence the rate of axial deformation were varied separately during the course of the experiment: axial stress (σ_1), temperature (25→50→77 °C), fluid composition, and injection rate (Fig. 5a). The wet deformation of the sample was initiated with the injection of pure water, followed by saline fluid (0.5 M NaCl + 0.05 M $MgSO_4 \cdot 7H_2O$), and terminated with propanol. After each period of fluid injection (injection at variable rates; median rate 0.1 ml/min), fluid flow was stopped over extended periods of time to allow for the establishment of steady-state deformation rates. The total duration of experiment L16 was 691 days.

The experimental parameters for expt. L9-11 were slightly different (Fig. 5b). The initial pressure loading of the sample under dry conditions (0-0.08 days) was followed by deformation in the presence of pure water (σ_1 = 4.9±0.1 MPa, σ_3 = 4.0±0.1 MPa, injection rate: 0.5, 0.2 ml min^{-1}). After the rate of deformation stabilized (over $t \approx$ 30-40 days), σ_1 was increased to 6.9±0.1 MPa (water injection rate: 0.2, 0.1 ml min^{-1}). Before the attainment of steady-state deformation, the temperature was increased from 25 to 50 °C, and the injected fluid was changed from water to saline solution (t ≈ 82 days and 90 days, respectively; fluid injection rate: 0.1 ml min^{-1}). The experiment was terminated during a regime with a "steady-state" rate of deformation at t = 120 days. The chemistry and pH of the exit fluids were semi-continuously measured. As opposed to experiment L16, fluids were continuously injected into the sample, without intermittent periods of zero flow.

4. RESULTS AND DISCUSSION

4.1. General Observations

4.1.1. Dry vs. fluid-assisted deformation; "steady-state" deformation

The pressure loading of all samples resulted in an initial period of dry deformation. As an example, Fig. 6 shows the preliminary deformation of sample L16 in the absence of fluids (note: Fig. 6 is a partial enlargement of Fig. 5a, which shows the entire deformation history of L16). The strain vs. time curve shows that the initial deformation rate of the sample rapidly decreases, to the point where $\dot{\varepsilon} \approx 0$. The total axial strain (ε) associated with dry deformation for experiment L16 is on the order of 0.005. This compaction is purely mechanical and can be attributed to crushing of grains at the end of the sample when the piston seats itself during loading. There may also be a small contribution due to partial pore collapse within the sample; however, pore collapse in dry chalks is generally attributed to much higher stresses, on the order of at least 10-20 MPa (the minimum amount of stress depends on the nature of the chalk, its porosity, amount and chemistry of pore fluids, etc.; e.g., Schroeder 1995; Pecqueur et al., 1995). The results in this study show no evidence for measurable steady-state deformation under dry conditions after the initial phase of mechanical compaction. On the other hand, the injection of fluids always triggered rapid deformation. Deformation associated with fluids is not transitory, but is a long term, time-dependent phenomenon (e.g., sample L16, t ≥ 12 days, Fig. 5a), suggesting a fluid-enhanced creep mechanism.

The fluids that were injected into the chalk cores were not pre-saturated with respect to calcite. On the other hand, exit fluids were saturated with respect to calcite, as determined by measurements of [Ca], the exit pH (9.1-9.8), and experimental data in the literature concerning calcite solubility (Plummer and Busenberg, 1982). Several lines of evidence show

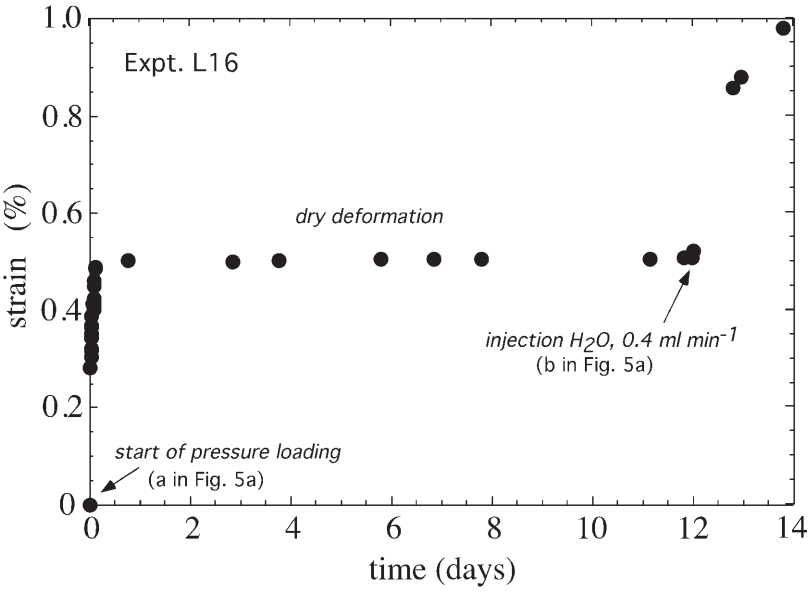

Fig. 6. Enlargement of Fig. 5a (note change in ordinate axis with respect to ε), showing rapid stabilization of initial dry deformation of L16 during stress loading. Long term, fluid-assisted deformation, which is attributed to pressure solution creep, is initiated with the injection of water into the sample.

that injected solutions become rapidly saturated with respect to calcite:

a. Exit calcium concentrations were invariant with respect to injection rate (e.g., change in injection rate from 0.025 to 0.007 ml min^{-1}).
b. Kinetic experiments of chalk in degassed H_2O and saline solution were performed and show that saturation with respect to calcite is achieved within ≤ 2 days at 20-25 °C. This is significantly less than the mean residence time of fluids in the chalk cores (> 4 days).
c. Studies in the literature confirm that the dissolution rate of calcite in water is very rapid at far from equilibrium conditions (log k = -6.63 mmol cm^{-2} s^{-1} at 25 °C; Busenberg and Plummer, 1986).

In referring to the general style of deformation behavior recorded in this study, initially rapid strain rates progressively stabilized with time, leading to local "steady-state" strain rates. The term local "steady state" refers to regimes of deformation where ε vs. t was approximately linear over periods of several tens of days (e.g., Fig. 9). True steady-state conditions ($\partial\varepsilon / \partial t = 0$) were never attained, even though at the end of some experiments the change in ε was too small to be measured (e.g., $t >$ 500 days, Fig. 5a). The stabilization of rates occurred when the experiments were configured both as open or closed systems (i.e., with and without flow- e.g., expt. L9-11, Fig. 5b).

4.1.2. Fluid chemistry behavior

When an aqueous fluid is first injected, or when the fluid injected is changed to one in which calcite is more soluble (e.g., water replaced by saline solution), there is always an initial rapid and transitory rate of deformation, accompanied by an elevated pulse of Ca in the exit solution (e.g., see 2 [Ca] spikes in Fig. 7; compare to deformation curves in Fig. 5b; both figures are based on expt. L9-11). In either case, the injection of fluid is predicted to lead to dissolution reactions at both free-face interfaces (i.e., grain surfaces in contact with pore space fluids) and stressed grain-to-grain interfaces. Both types of reactions are probably responsible (to varying degrees) for grain compaction and deformation of the matrix. Fluid access to pore spaces containing surface fines created by grain crushing during the initial phase of dry deformation may be the main reason for the behavior of Ca shown in Fig. 7 (i.e., [Ca] spike during first 20 days; [Ca] spike associated with injection of saline solution, $t >$ 90 days). In the same figure, the elevated, steady-state [Ca] ($t >$ 115 days) is a function of the increased solubility of calcite in the saline solution. In contrast to the behavior shown in Fig. 7, a change in fluid chemistry from high calcite solubility to lower solubility does not lead to a [Ca] spike.

The experimental results show that the exit solution chemistry is only nominally affected by changes in the

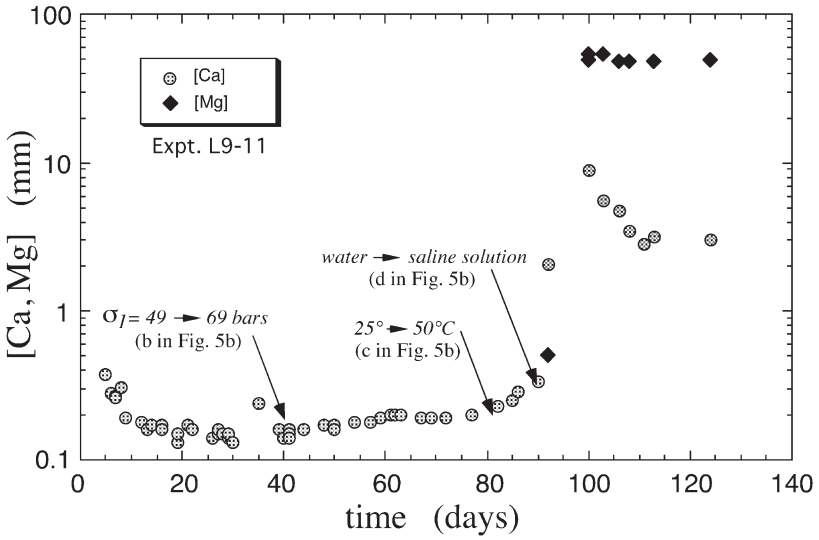

Fig. 7. Evolution of Ca and Mg content in output fluid, L9-11. Response of exit [Ca] to change in vertical stress is small, whereas changes in temperature and fluid chemistry significantly influence [Ca]. The magnitude of these changes is a function of calcite solubility. The response of $[Mg]_{exit}$ after the injection of Mg saline solution reveals that dispersion of fluids occurs within the matrix.

applied stress. The very small change in calcite solubility as a function of applied stress can be calculated using Eqn. 1b. A significant change in the vertical stress (several MPa) had no measurable effect on the exit solution [Ca] in most experiments; however, in some cases the effect was small, but nonetheless measurable. One such example is shown in Fig. 7, where [Ca] increases slightly due to a change in axial stress ($\sigma_1 = 4.9 \rightarrow \sigma_1 = 6.9$ MPa, $t > 40$ days). On the other hand, the aforementioned change in the axial stress induces a large increase in the strain and the strain rate, as can be seen in Fig. 5b. The various examples discussed above reveal an important point: the behavior of [Ca] in the exit solution does not correlate in a simple manner with changes in the deformation rate.

4.1.3. Fluid flow effects

Even though the influence of fluid flow on deformation rates was not explicitly studied in the present study, the effect was not overly significant. In general, when the experimental configuration was changed from open to closed conditions, there was no measurable effect that could be differentiated from the evolution of the 'background' compaction rate (i.e., stabilization). In one case in particular, however, there was a measurable effect when the system was changed from closed to open conditions: the steady-state rate of deformation (at t = 400 days, expt. S17) jumped from 2.4 x 10^{-10} to 4.8 x 10^{-10} s^{-1} when fluid flow was induced at υ = 0.5 ml $mins^{-1}$; the latter rate stabilized to 1.5 x 10^{-10} s^{-1} after a period of approximately 100 days. The sudden increase in the deformation rate may have been the direct result of an increase in the importance of free-face dissolution (due to a higher degree of pore fluid undersaturation), this resulting in undercutting of grains and matrix deformation.

The effect of fluid flow on deformation rates may vary, depending on the process that is rate-limiting. In the current experiments, the dependence was in most cases difficult to quantify and not significant. On the other hand, a study of the deformation of wet gypsum aggregates showed increases in the rate of compaction creep by a factor of 10-30x with fluid flow (de Meer and Spiers, 1997); this behavior was attributed to precipitation in pore spaces being the inferred rate-limiting step. Based on the above example, it is evident that fluid flow may change the rates of pressure solution deformation. For this reason, when examining strain vs. time data in experimental studies such as these (e.g., Figs. 5a, b), it is important to exclusively use values of $\dot{\varepsilon}$ that are derived from steady-state ε vs. time curves at conditions of zero fluid flow; this increases the probability that the fluids in the interconnected pore spaces are saturated (with respect to calcite in present study), such that measured deformation rates are a function only of pressure solution reactions (intergranular and/or free-face).

4.2. Overview of Rate-Determining Parameters

4.2.1. Constitutive relations

As was previously discussed, the current literature contains numerous models describing pressure solution deformation of geological materials. A brief discussion concerning an intergranular pressure solution model is presented in order to qualitatively analyze the various deformation rate-influencing parameters based on the present results. The constitutive relations developed by Rutter (1976) and Dewers and Ortoleva (1990a, 1990b) can be used as a representative example. Their models are based on diffusion in the trapped intergranular fluid being the rate-controlling step; a condensed version that was applied to quartz aggregates (Eqn. 7, Dewers and Hajash, 1995) shows that the strain rate ($\dot{\varepsilon}$) can be expressed in terms of the following parameters:

$$\dot{\varepsilon} = \frac{k' C^{eq}}{d^n (1-\varepsilon) A_D} \left\{ \exp(\alpha' P_e f) - 1 \right\} \quad (4)$$

where k' is a thermally-activated diffusion coefficient, C^{eq} is the solid solubililty at fluid P and T, d is the initial grain diameter (with $n = 1$), ε is the strain, A_D is the area of contact (equivalent to square of island diameter), α' is a temperature and molar volume-dependent coefficient, P_e is the effective stress, and f is a stress magnification term for relating the far field stress to mineral grains. The stress magnification term f is not a constant since it decreases as a function of increasing strain, such that the effective stress decreases as well, thereby causing the rate of strain $\dot{\varepsilon}$ to decrease with ongoing compaction. Considering d and A_D as constants is an approximation since they will increase during compaction, which in turn decreases the local stresses and the rate of strain $\dot{\varepsilon}$. The use of ε in constitutive equations is avoided by some workers in the field, who instead use porosity which is considered a state variable. However, the use of ε has the advantage that it is a directly measurable quantity during deformation, whereas porosity is not.

Equation 4, which contains most of the fundamental rate-determining parameters that are associated with pressure solution, can be used as a guide for examining the experimental results from the present study, based on data from a total of 9 experiments, including L9-11 and L16. A much more detailed analysis of these data, in the context of constitutive relations as well as the mechanisms of pressure solution, is the subject of a forthcoming communication (Hellmann et al., in prep.).

4.2.2. Effective stress

In the present study, it was assumed that the measured vertical strain is accommodated by mass transfer from the grain contacts perpendicular to σ_1 to free faces associated with pore spaces containing pore fluid at pressure P_f. For this reason, the effective stress has been defined as: $\sigma_{eff} = \sigma_1 - P_f \approx \sigma_1$; the effect of the pore pressure (in connected pore spaces) was neglected since it generally did not exceed ≈ 0.3 MPa at the inflow end of the core. In one experiment (S8-9), however, the effect of the pore pressure was investigated. A change in the pore pressure from 2.0 to 0.5 MPa (measured and controlled at the outflow end by the backpressure regulator, constant injection rate of 0.007 ml min^{-1}, σ_1 = 8.8 MPa) resulted in a sudden and transitory increase in the rate of deformation, followed by rapid stabilization. The steady-state strain rates before and after the pressure decrease were approximately the same.

The relation between the strain rate and the effective stress was determined by plotting $\dot{\varepsilon}$ vs. σ_1 in log-log space ($\dot{\varepsilon}$ at constant T, ε, chemistry of solutions). The instantaneous strain rates were based on tangents to strain-time curves (i.e., $\partial l / \partial t$ in Eqn. 3). The resulting slopes, in the majority of cases, ranged from 1-2. This range in values appears to be normal for pressure solution experiments at moderate effective stresses. As a comparison, Spiers et al. (1990) determined slopes of ≈ 0.8-1.8, based on the densification of salt at $\sigma_{eff} \leq 2.1$ MPa; at higher σ_{eff} (> 4 MPa), the dependence of $\dot{\varepsilon}$ on σ_{eff} was much higher, with slopes ranging from 2-4. Creep experiments using wet gypsum aggregates (de Meer and Spiers, 1995, 1997) produced slopes of ≈ 1.5-3.5. An investigation of the pressure solution deformation of quartz sand at 200 °C (Dewers and Hajash, 1995) also showed a large variation in slopes, ranging from 0.2-2.65 (based on linear slope segments in log $\dot{\varepsilon}$ - log σ_{eff} space, $7 < \sigma_{eff} < 48$ MPa). Based on all of the above data (except that of gypsum), it appears that there is quasi-linear relation between $\dot{\varepsilon}$ on σ_{eff} at low effective stresses; this has been pointed out by Rutter (1976), for example, who developed a constitutive relation based on $\dot{\varepsilon} \propto \sigma_{eff}$ at low effective stress values ($\sigma_{eff} < 30$ MPa). Nonetheless, beyond a certain critical limit in effective stress (which is dependent on the material, ε, T , etc.), the linear relation between $\dot{\varepsilon}$ vs. σ_{eff} gives way to a power law or exponential relationship, which appears to be compatible with the $\dot{\varepsilon}$ vs. σ_{eff} relationship given in Eqn. 4.

The relation $\dot{\varepsilon} \propto A\sigma_{eff}^m$, where A and m are constitutive parameters, is useful in elucidating the mechanisms of deformation. Solids displaying Newtonian rheological (viscous) behavior, by definition, are characterized by $m = 1$. Low values of m are typically related to diffusional transfer processes (Evans and Kohlstedt, 1995), such as Nabarro-Herring creep (matrix diffusion), Cobble creep (grain boundary diffusion), or pressure solution creep (dissolution and

fluid diffusion in grain boundaries). However, values of $m > 2$ are commonly reported for pressure solution at elevated stress values. Whether this change in m is strictly linked to the influence of stress on solubility (as in Eqn. 4) or to evolution towards another deformation mechanism is not yet clear. For example, m = 3 or 5 is attributed to crystalline plasticity or creep via dislocation movement (see original references in section 4, Evans and Kohlstedt, 1995).

4.2.3. Grain size

According to most models in the literature where diffusion in the intergranular regions is the rate-limiting step, the strain rate varies inversely with the cube of the radius of the grains: $\dot{\varepsilon} \propto 1/d^{n=3}$. (Raj, 1982; Rutter, 1983; Lehner, 1990; Spiers and Brzesowsky, 1993). On the other hand, if interfacial kinetics are rate-controlling, the strain rate simply varies inversely with radius, and $n = 1$ (Raj, 1982). In Eqn. 4 the former relation between strain rate and grain size is implied (i.e., $n = 3$), but not explicitly formulated, due to the separate d and A_d terms. Halite densification data from Spiers and Brzesowsky (1993), for example, confirm the relation $\dot{\varepsilon} \propto 1/d^3$, indicating pressure solution creep rates limited by diffusion. In contrast, pressure solution experiments on wet gypsum aggregates yielded variable results, with $n \approx$ 1 (de Meer and Spiers, 1995) and $n \approx$ 2-4 (de Meer and Spiers, 1997). A quartz sand study by Dewers and Hajash (1995) showed that $\dot{\varepsilon} \propto 1/d^{2.3}$. Since there was no way to systematically vary the grain size in the chalk cores in the present study, the dependence of the strain rate on grain diameter could not be determined. In Eqn. 4, the diffusion parameter k (which includes the diffusion coefficient D and the width of the intergranular fluid film w), which in general cannot be measured directly, was not evaluated in the present study.

4.2.4. Strain and strain hardening

It is important to note that periods of deformation termed "steady-state" are not truly invariant with time. Taking an example from Fig. 5a, based on a regime of "steady-state" deformation in the presence of water (σ_1 = 6.0 and σ_3 = 4.0 MPa, T = 50 °C, zero fluid flow), the strain rate ($\dot{\varepsilon}$) decreases almost an order of magnitude with increasing time and compaction (ε), from 2.71 x 10^{-10} s^{-1} (ε = 0.0160, t = 78.20 days) to 3.62 x 10^{-11} s^{-1} (ε = 0.0178, t = 144.55 days). Based on an extrapolation of this strain vs. time data to 700 days, ε = 0.0185 and $\dot{\varepsilon}$ = 7.24 x 10^{-12} s^{-1} are predicted. This demonstrates that even over very long time periods (at least with respect to laboratory time scales), apparent "steady-state" rates of wet chalk deformation continue to evolve with time and therefore, $\dot{\varepsilon}$ is never constant. This strain hardening behavior demonstrates that the influence of strain on strain rates over long periods of time is not negligible, and hence, the term "steady-state" strain rate is actually only a valid approximation over small (local) time intervals, extending not more than a few tens of days.

In the constitutive relation given by Eqn. 4, the effect of the strain on strain rates is given by $\dot{\varepsilon} \propto 1/(1-\varepsilon)$. The strain magnification term (f in Eqn. 4) also influences the stress as a function of the strain. A constitutive relation developed by Spiers and Brzesowsky (1993) for salt aggregates is based on an inverse relation between the volumetric strain rate ($\dot{\beta}$) and strain (ε), such that $\dot{\beta} \propto 1/\varepsilon^c$ (note that $\dot{\beta} = 3\dot{\varepsilon}$). According to their experimental data, $c \approx 2$ for strains up to 10%, and $c \approx$ 4-5 for strains of 15-20% (Spiers et al., 1990, Spiers and Brzesowsky, 1993). Thus, the inverse dependence of the strain rate on strain is much greater in their model than that proposed in Eqn. 4. In a similar manner, two gypsum aggregate studies yielded highly variable values, with c ≈ 4.3-7.5 (from Fig. 3, de Meer and Spiers, 1995), but were much lower in a latter study using gypsum, with c ≈ 2.4-4.2 (from Fig. 3, de Meer and Spiers, 1997). Quartz sand compaction rates measured by Dewers and Hajash (1995) showed a much smaller dependence on strain, with $\dot{\varepsilon} \propto 1/(1-\varepsilon)$, which is equivalent to the relation in Eqn. 4. In the present study, the dependence of the axial strain rate on strain (constant T, σ_1, chemistry of solutions) yields values of $c \approx$ 2-5. The range in c reflects both experimental scatter and the heterogeneous deformation behavior of the chalk; nonetheless, this result shows the strong inverse dependence of the rate of deformation on strain. At first glance, comparing the above results for halite, quartz, and chalk compaction suggests that the solubility of the material may affect the dependence of the strain rate on strain and the strain hardening behavior. The different dependencies of $\dot{\varepsilon}$ on σ_{eff} may also result from different assumptions concerning the fundamental mechanisms of pressure solution (see discussion in Dewers and Hajash, 1995).

4.2.5. Chemistry of solutions

The effect of solution chemistry, which controls the solubility of chalk, is given by the C^{eq} term in Eqn. 4. In fact, most intergranular pressure solution models in the literature generally incorporate a linear dependence of the strain rate on the non-stressed solubility of the solid (see Eqn. 1d). This follows from the fact that most *ips* models equate the strain rate with the outward flux of dissolved material, which is a function of the concentration gradient.

A few studies have examined the effect of solution chemistry on strain rates. A study by Rutter (1976) showed that 3 salts were found to deform at rates qualitatively in accord with their solubilities, as predicted by Eqn. 4. A gypsum study by de Meer and Spiers (1997) showed that aggregates flooded with oil, which is a non-polar solvent, showed no measurable creep. Studies concerning the mechanical behavior of chalks also show that the chemical nature of the fluid strongly affects the yield strength (see section *4.3.1* below). As an example, triaxial tests using saturated chalk samples demonstrated that the salt content of aqueous fluids is directly related to the degree of weakening of the chalk (Da Silva et al., 1985; see Figs. 4-6 therein).

In the present study, the effect of solubility was investigated by changing the chemical nature of the fluid (water vs. Mg-saline solution, polar vs. non-polar solvent). The results show that chalk deformation rates are a strong function of the fluid chemistry. In comparison to calcite solubility in pure water, calcite is more soluble in the saline solution used, and less soluble in propanol (the changes in solubility are approximately one order of magnitude with respect to pure water). The influence of solution chemistry on the deformation behavior of chalk for expts. L16 and L9-11 was investigated by changing the chemical composition of the injected fluids several times (water → saline solution → propanol).

The first change in chemistry involved the replacement of water by the injection of a saline solution ("d" in Figs. 5a and b). The non-steady-state deformation behavior is characterized by an abrupt increase in the strain and strain rate, followed by a stabilization of the strain rate (Figs. 5a, b, and 8a). The change in deformation behavior is due to the higher solubility of calcite in saline solution vs. water. To quantify the effect of chemistry on steady-state strain rates, we examine the switch from water to saline solution in L16 (Fig. 5a, ε vs. time data on both sides of point "d"). The steady-state $\dot{\varepsilon}$ in water is ≈ 3.62 x 10^{-11} s^{-1} (ε = 0.0178, t = 144 days, zero flow); after the switch to saline solution, $\dot{\varepsilon}$ ≈ 6.03 x 10^{-11} s^{-1} (ε = 0.0189, t = 260 days, zero flow). However, a meaningful comparison of $\dot{\varepsilon}_{water}$ *vs.* $\dot{\varepsilon}_{saline}$ must be made for the same strain (see discussion concerning strain hardening). One way this can be determined is by extrapolation of the $\dot{\varepsilon}_{water}$ vs. t curve forward in time, up to the point where ε = 0.0189; this results in $\dot{\varepsilon}$ ≈ 2.78 x 10^{-12} s^{-1}. Thus, comparing the two strain rates at the same strains reveals the dramatic effect of the solution chemistry: $\dot{\varepsilon}_{\text{saline}} \approx 20\,\dot{\varepsilon}_{\text{water}}$.

The second change in chemistry that is examined concerns L16 and a switch from saline solution to propanol. The effect that injection of a non-aqueous (non-polar) solvent, propanol, has on the rate of deformation is shown in Figs. 5a (point "h") and 8b (an enlargement around point "h"). In this case, the effect on the deformation rate is the opposite, the axial strain rate diminishes to the point where $\dot{\varepsilon}$ is no longer measurable (making a quantitative comparison of strain rates impossible). The drastic reduction in the strain rate is due to the very low solubility of calcite in propanol, a non-polar solvent.

The dependence of $\dot{\varepsilon}$ on the chemical nature of the fluid (solubility of solid) measured in the present study supports the relation $\dot{\varepsilon} \propto C^{eq}$ that is expressed in Eqn. 4. However, whether this relation is perfectly linear remains to be determined. Perhaps the most important implication of these results is that they offer additional evidence that pressure solution creep of chalk (and other materials) is not solely a mechanical process, but also depends on chemical reactions and transport processes occurring in intergranular interface regions.

4.2.6. Temperature

Temperature was the last parameter investigated. An increase in temperature has two main consequences with respect to the rate of pressure solution and chalk deformation. Since calcite solubility decreases with temperature (due to retrograde solubility), the solubility term acts to decrease the strain rate with increasing temperature. On the other hand, the rate of diffusion, D, increases with temperature. The temperature dependence of D can be expressed in terms of the Arrhenius relationship, $D \propto \exp(-E_a / RT)$, where E_a is the activation energy and R is the universal gas constant.

Diffusional processes generally have a weak dependence on temperature as a consequence of low activation energies. In the present study, an increase in temperature by several tens of °C always resulted in an abrupt and significant increase in $\dot{\varepsilon}$, followed by the establishment of a steady-state rate of deformation that was just slightly higher than the original, lower temperature rate (see Fig. 5a- point "f", Fig. 5b-point "c", and Fig. 9). Applying the Arrhenius relationship to deformation rates (i.e., plotting log $\dot{\varepsilon}$ vs. $T(\mathrm{K})^{-1}$) results in a preliminary estimate of ≈ 1-2 kJ mol^{-1} for E_a, using data from one experiment (S17) where the temperature was raised sequentially from 25 to 60 to 80 °C (Fig. 9). This estimate is based on rates of deformation that were normalized to the same strain; however, the rates were not normalized with respect to solubility as a function of temperature.

This estimate can be compared with activation energies in the literature. A study of grain boundary diffusion under wet conditions determined an activation

energy of 15 kJ mol^{-1} (Nakashima, 1995). Two studies based on salt pressure solution yielded higher activation energies: 19 kJ mol^{-1} (KCl, Pharr and Ashby, 1983) and 24 kJ mol^{-1} (NaCl, Spiers et al., 1990). On the other hand, a study by Hickman and Evans (1995- see description in *Introduction*) found no temperature dependence. Nonetheless, as Hickman and Evans (1995) point out, great care must be taken when comparing pressure solution activation energies in the literature. In addition, many estimates of E_a are based on strain rate-temperature data which include not only the effects due to the thermal activation of diffusion, but also the effects of temperature on solubility; this is the case for the estimate from this study, for example.

The weak dependence of strain rates on temperature reflects the low E_a associated with diffusional processes in a fluid (E_a < 20-30 kJ mol^{-1} for diffusion-controlled kinetic processes; e.g., Lasaga, 1981). This implies diffusional transport in intergranular fluids, and not just in pore fluids. Not all studies have found low activation energies, however; Dewers and Hajash (1995) determined an activation energy of 73 kJ mol^{-1} for quartz sand compaction. This value is the same as that measured for quartz dissolution. This high activation energy indicates that for the case of quartz sand pressure solution, dissolution rather than diffusion should be the rate-determining step, at least to moderately elevated temperatures.

4.3. Fluid Flow and Interactions with Chalk Matrix

4.3.1. Fluid percolation behavior

The penetration of fluids into the matrix of samples is important for understanding the dynamics of fluid flow, fluid communication between pore spaces, as well as intergranular chemical interactions. Results from experiment L9-11 show (see Fig. 7), for example, how the output chemistry changes as a function of time when water (calcite-saturated) is replaced by Mg-bearing saline fluid (constant injection rate of 0.1 ml min^{-1}, theoretical Darcy velocity ≈ 0.0032 cm min^{-1}, total pore space volume ≈ 628 cm^3, avg. porosity ≈ 40%, 20 cm. core length). After switching from water to Mg-saline solution, the first Mg signal in the exit fluid is recorded after ≈ 2.1 days. The time necessary for [Mg] in the exit solution to match the [Mg] of the input solution is ≈ 9.8 days. Plotting $[Mg]_{exit}$ / $[Mg]_{input}$ vs. time results in what is termed a cumulative residence-time distribution curve *F(t)*; analysis of this *F(t)* curve (see details in Denbigh and Turner, 1984) yields a mean residence time of ≈ 5 days. On the other hand, based on an average porosity of 40%, and assuming that all pore spaces are accessible to the injected fluid and that pore spaces fill at an equal rate from bottom to top in the core, an injection rate of 0.1 ml min^{-1} corresponds to a theoretical residence time of ≈ 4.3 days. This situation corresponds to a chalk core that behaves as a plug flow reactor with no internal dispersion, such that a step change in the input chemistry remains a step change at the exit of the core. The behavior of the measured Mg *F(t)* curve (i.e., spread of *F(t)* about the mean) indicates that dispersion occurs within the chalk, such that some fluids bypass a significant portion of the matrix, whereas others percolate much more slowly. This indicates that a portion of the fluid flow is localized in channels and zones of enhanced porosity (e.g., Fig. 2 - Part 2), whereas the remaining fluid flow infiltrates the micropore space structure over much longer time scales (t > 10 days for the above conditions) than the mean residence time.

It is interesting to note that changes in the chemistry of the injected fluid do not induce an immediate change in $\dot{\varepsilon}$, but rather $\dot{\varepsilon}$ changes after a time lag. Based on several experiments where the fluid chemistry was changed, the time lag is variable, depending on the injection rate, the nature of fluid replacement (polar vs. non-polar), as well as such factors as the strain; two examples illustrate the influence of the two latter factors. The first example concerns the replacement of water by Mg-saline solution (two polar fluids) at a constant injection rate of 0.1 ml min^{-1} (point "d" - Fig. 5b, expt. L9-11). The strain vs. time curve (Fig. 8a) shows a modest increase (perturbation) in the strain rate ≈ 2.5 days after the injection of saline fluid, followed by a gradual stabilization of the rate. The second example that is discussed differs from the first in that Mg-saline fluid, which has a polar nature, is replaced by propanol, which is much less polar (point "h"- Fig. 5a, expt. L16; replacement at constant injection rate of 0.1 ml min^{-1}). As can be seen more clearly in Fig. 8b, the time lag associated with a measurable change in the strain rate is much greater, on the order of weeks. The difference in the response rates in these two examples is most probably a function of two variables: first, the difference in the polar nature of the injected fluid vs. the in-situ pore fluid, and second, the differences in the strain at the time of injection (0.0142 in expt. L9-11 and 0.0282 in expt. L16). The influence of the first factor can be attributed to the fluid's wettability characteristics; in addition, the miscibility of both fluids may also play a role. The second factor, the degree of strain, influences the porosity and permeability, which in turn controls the rate of access of injected fluids into pore spaces.

When a change in the fluid chemistry is effected, the rate of infiltration of new fluids into the micro-pore space matrix occurs over very long time scales, on the order of days to weeks (with respect to the two examples discussed earlier). The first measurable changes in strain rates most probably occur when only a fraction

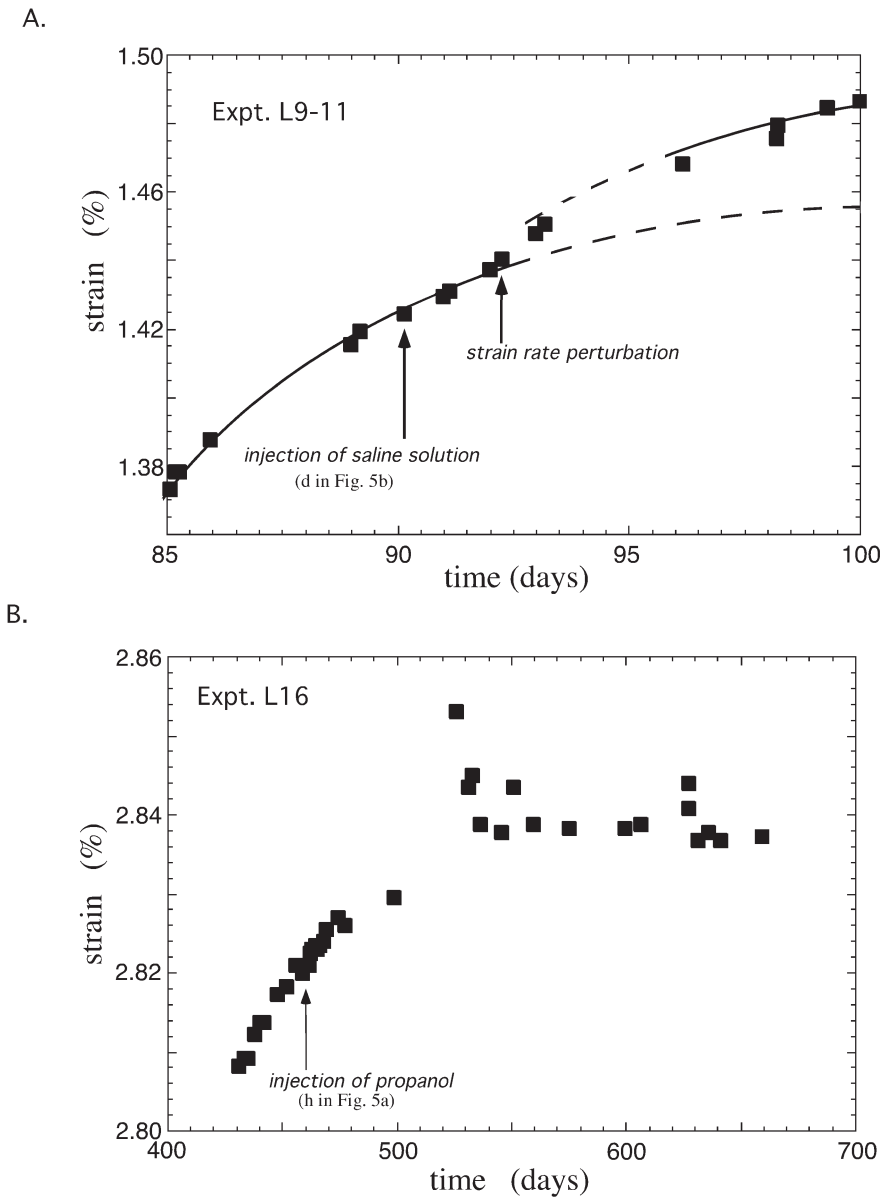

Fig. 8. Evolution of strain as function of chemistry of input solution. (A) Replacement of water by saline fluid results in an increase in strain rate, due to an increase in the solubility of chalk in saline solution. (B) Replacement of saline solution by propanol significantly decreases the rate of deformation, due to the low solubility of chalk in propanol. Excursions of data at $t > 500$ days due to unknown reason.

of the pore spaces have had their fluids exchanged, as estimated from cumulative residence time curves. As time progresses, strain rates continuously adjust to the saturation of all of the pore spaces with the injected fluid. It is, nonetheless, difficult to estimate what percentage of pore spaces is initially affected and the rate at which complete pore saturation occurs. Because of the continual compaction of the chalk, it is also difficult to deconvolute the effects of fluid chemistry changes with those due to increasing strain and compaction, especially since they operate in an inverse manner with respect to the strain rate (see Eqn. 4).

For a change in solution chemistry to affect the overall pressure solution process, not only must fluids infiltrate all of the pore spaces, but in addition, a diffusional process must occur from pore spaces to the

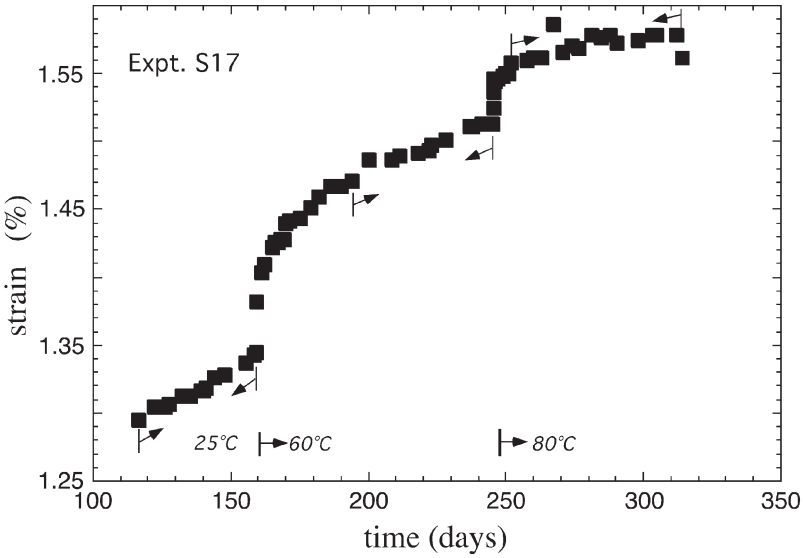

Fig. 9. Evolution of strain with increases in temperature; note the rapid changes in strain rate, followed by stabilization (local "steady states" delimited by arrows). Based on this data and the Arrhenius equation, the estimated activation energy is very low: ≈1-2 kJ mol^{-1}.

intergranular regions at stressed grain-to-grain contacts. However, the rate at which fluids penetrate and wet stressed grain-to-grain boundaries is uncertain, especially since the rates of diffusion in thin, trapped fluid films remain one of the biggest uncertainties with respect to the pressure solution mechanism. An additional complication arises from the fact that the progressive replacement of one fluid by another at stressed contacts requires the diffusion of aqueous species in the opposite direction with respect to the diffusion of dissolved material from intergranular regions to pore spaces (refer to Fig. 2); this raises the question whether the inward and outward diffusion of species are possibly coupled (note: coupled diffusion processes occur in a variety of geochemical processes, for example, the formation of leached layers in certain minerals and glasses- see e.g., Hellmann, 1997; and references therein). Fluid miscibility may also be an additional factor of importance with respect to the rate of exchange of fluids in pore spaces and intergranular regions.

To summarize the fluid percolation behavior in the present study, the slow response of strain rates (days to weeks) to changes in fluid chemistry is evidence that the deformation behavior of chalks is controlled primarily by intergranular reactions, and not rapid dissolution of free-face interfaces that are in contact with pore space fluids (refer to discussion on mechanisms of pressure solution). Free-face dissolution reactions in pore spaces should lead to changes in deformation rates with response times not longer than the mean residence times of fluids in the chalk cores; this estimate is based in part on the kinetics of chalk dissolution under isotropic conditions.

4.3.2. Chemical nature of fluids: mechanical vs. chemical effects

Because of the importance of oil reserves in chalk reservoirs (e.g., North Sea), many recent investigations have aimed to understand the role of different types of fluids in chalks, especially in terms of their ability to penetrate pore spaces and the effect they have on their mechanical strength. Among the key properties studied have been the wettability of interfaces and capillary forces (e.g., Andersen et al. 1992; Piau and Maury, 1994, 1995; Brignoli et al., 1995; Schroeder, 1995; Delage et al., 1996; Homand et al., 1998; Schroeder et al., 1998; Risnes and Flaageng, 1999; and references therein); these two properties are a function of the dielectric constant, the polarity, and the surface tension of the fluid.

Delage et al. (1996) and Schroeder and Shao (1996), for example, determined that the polar nature of the fluid affects the mechanical resistance of chalk; their results show that the upper limit of elastic deformation behavior (yield strength) is dependent on the nature of the pore fluid, and increases in the following order: seawater < water < methanol < oil, dodecane < absence of fluid. In quantitative terms, it was determined that

the pore collapse threshold (i.e., this corresponds to the upper limit of elastic behavior) occurs at 5-7 MPa in water-saturated chalk samples (Schroeder, 1995) and 10-15 MPa in paraffin or kerosene-saturated samples (Delage et al., 1996). Delage et al. (1996) and Schroeder and Shao (1996) reason that chalks containing oil or dodecane are stronger than those containing seawater or water because of capillary effects, where the attractive forces between grains are due to menisci formed by connate water bridges between grains (Schroeder et al., 1998; Homand et al., 1998). Fluids that have a high wettability potential (e.g., water, seawater, and similar polar fluids) tend to decrease local capillary attraction between grains by destroying grain-to-grain menisci, which destabilizes the grain structure and results in pore collapse. Apparently when a non-polar fluid (oil) is replaced by a polar fluid (water), the transition from oil-saturated behavior (high mechanical resistance) to water-saturated behavior (lower mechanical resistance) is abrupt; 2% water saturation is sufficient for chalk to behave as if it were completely water-saturated (Schroeder et al., 1998).

Another series of tests concerning the mechanical strength of chalks was carried out with varying methanol-water mixtures (Risnes and Flaageng, 1999). Their study measured a monotonic increase in the yield strength of chalk (11 to 18 MPa, based on compression tests) as the mole % of methanol was varied from 0-100%. Risnes and Flaageng (1999) propose two mechanisms to explain their results: 1. water weakening of silica cement bonds within the chalk matrix 2. development of repulsive forces of electrostatic origin between grains (measured zeta potential values of chalk powder: water = -20mV, methanol = +10 mV, oil ≈ 0 mV).

It is interesting to note that the order of fluids with respect to increasing mechanical resistance of chalk (see above, Delage et al., 1996 and Schroeder and Shao, 1996) follows qualitatively the solubility of chalk in these fluids, in decreasing order; in other words, the mechanical strength varies inversely with solubility. Based on the results in the present study and many other pressure solution models, the rate of deformation is proportional to the solubility (see Eqn. 4), such that chalk deforms at a much higher rate in the presence of seawater than in the presence of an alcohol, for example (see evidence for this in Figs. 8a, b). Thus, the overall effect of the chemistry of fluids on deformation behavior is similar between models based on capillary forces and pressure solution (i.e., as in the present study), the main difference being that the former is based on *physico-mechanical interactions* between grains, whereas pressure solution is based on *chemical dissolution reactions* in stressed intergranular regions.

4.3.3. Application of numerical model results: dissolution and precipitation in porous media

The dissolution and precipitation behavior of solutes in porous media and fracture systems has recently been examined in a series of numerical modeling studies (e.g., Sallès et al., 1993; Békri et al., 1995, 1997; Mourzenko et al., 1996). The results from these studies show that the geometry of pore and fracture spaces, as well as two associated dimensionless parameters, the Péclet and Péclet-Damköhler numbers, are important in the evolution of the hydrodynamic and chemical behavior of the system. The Péclet number (Pe) is a comparative measure of the convective vs. the diffusion characteristics of the system; Pe < 1 indicates diffusion is predominant, whereas convection predominates when Pe > 1. The Damköhler number (Da) is a comparative measure of kinetics (rates of dissolution or precipitation) vs. convection; when Da < 1 convection predominates, and for Da > 1, kinetics predominates. Finally, the Péclet-Damköhler number is a measure of kinetics vs. diffusion, such that if PeDa < 1, diffusion is more rapid and therefore the process is reaction rate-limited, and conversely, when PeDa > 1, kinetics are more rapid, such that diffusion is rate-limiting. The respective definitions of Pe, Da, and PeDa, as applied to porous media, are defined as follows:

$$\mathrm{Pe} = \frac{\bar{v}_0^* b_m}{D}; \qquad \mathrm{Da} = \frac{K}{\bar{v}_0^*}; \qquad \mathrm{PeDa} = \frac{K b_m}{D} \quad (5)$$

where $\bar{v}_0^*$ is the average interstitial velocity in the porous medium (or fracture), b_m is the initial aperture opening of the pore space or fracture, K is the kinetic rate constant, and D is the coefficient of diffusion (Mourzenko et al., 1996). The fluxes associated with either dissolution or precipitation at a connected pore space or fracture wall have been related to the interfacial solute concentration by PeDa (Békri et al., 1995, 1997). According to the results of Sallès (1993) and Békri et al. (1995), when PeDa < 1, precipitation is reaction-limited and occurs uniformly throughout the medium; on the other hand, if PeDa > 1, precipitation is predicted to occur either in the widest parts of pore spaces (Pe < 1) or along the main flow paths (Pe > 1).

In the present study, Pe was very small, on the order of 10^{-4}, based on $b_m \approx 1$ μm, $\bar{v}_0^* \approx 10^{-7}$ m s^{-1}, and $D \approx 10^{-9}$ m^2 s^{-1}. The determination of PeDa is more difficult, since the rate of precipitation (K) is not known. However, K is with certainty < 10^{-3} m s^{-1}, such that even if an exact value cannot be determined, PeDa << 1. According to the numerical results discussed immediately above, this corresponds to a situation of uniform precipitation throughout the matrix. This predicted result has relevance to the present

study with respect to the high density/low porosity zones observed in the interfacial regions of L9-11 and L16. The CT image in Fig. 16-Part 2 (and Fig. 18-Part 2 to a lesser degree) does show a uniform zone of high density which can be attributed to precipitation. The localized nature of these zones, as well as their positions, cannot however be predicted with the models discussed above. Despite the mathematical complexity of these numerical approaches, precipitation processes are dependent on many critical factors that have not been incorporated, such as kinetic and nucleation parameters.

5. CONCLUSIONS

Chalk subjected to moderate levels of differential stress in the presence of fluids undergoes time-dependent deformation and compaction that can be primarily attributed to pressure solution creep. The strain and the derived strain rates were measured as a function of several variables: effective differential stress, strain, solubility of the solid, and temperature. The linear relationship between the strain rate and vertical stress (in log-log space, with slopes $m \approx 1$-2) and the direct influence of the chemistry of the fluid on the rate of deformation strongly support a pressure solution mechanism. The inverse relation between the strain rate and the strain points out that time-dependent strain hardening is an important experimental parameter during the compaction of porous materials such as chalk. The dependence of the deformation rate on temperatures is very weak (measured up to 80 °C in the present study). The chemical nature of chalk deformation, based on pressure solution creep, is a concept which has been largely ignored in most mechanical models of chalk deformation. Perhaps one of the most important contributions of this study is to enlarge the debate concerning the nature of chalk deformation mechanisms.

While the long-term creep behavior of chalk points to a pressure solution mechanism, it is possible that this mechanism is assisted by others when the chalk-fluid 'system' is perturbed (i.e., non-steady-state behavior). As shown by the strain vs. time curves in the present study, the strain rates nearly always changed in an abrupt manner after a change in temperature, solution chemistry, or effective stress. These periods of rapid deformation were always transitory, since they gave way to very slowly varying, time-dependent creep (often referred to as "steady-state"). The rapid and very transitory nature of these perturbations may be related to grain-grain sliding, due to the partial dissolution and subsequent breakage of cement bridges connecting the grains. The loss of cohesion of cement bridges can be envisioned to be a physico-chemical process, where rapid free-face dissolution of bridges leads to mechanical failure and concomitant grain-grain sliding. In natural systems, rate-influencing parameters should not be subject to rapid changes, such that pressure solution creep should be the dominant deformation process at moderate levels of stress in wet chalks. However, rapidly applied external perturbations may be pertinent under some conditions, such as associated with oil exploitation operations in chalks (e.g., North Sea) or also with certain tectonic conditions (e.g., seismic activity, pulsed fluid flow in fault planes). In such cases, transient strain rate jumps are potentially a function of multiple deformation mechanisms, such as pressure solution creep, grain-grain sliding, brittle failure, and perhaps other modes of deformation, as well. The partitioning of strain among these modes of deformation merits additional study.

Acknowledgements—This research was supported by generous grants from Elf Aquitaine (Pau, France) and the GdR-Géomécanique program (CNRS). Comments from M. Jessell, C. Schroeder, F. Renard, and A.-M. Boullier aided in clarifying certain points in the original manuscript. We thank Brian Evans, Enrico Merino, and Andrew Hajash for their constructive reviews of the manuscript (note: the original reviews were based on a single manuscript, before it was divided into Parts 1 and 2; however, the scientific content and interpretations remain unchanged). R.H. also thanks Brian Evans for assuming the task of editorial handling.

Finally, I would like to acknowledge David Crerar's role as teacher, advisor, and friend during the 6 years of my graduate studies in his geochemistry group in the Department of Geology and Geophysics, Princeton University. -Roland Hellmann

Editorial handling: Brian Evans

REFERENCES

Andersen M. A., Foged N., and Pedersen H. F. (1992) The link between waterflooding-induced compaction and rate sensitive behavior in a weak North Sea Chalk. *4th North Sea Chalk Symposium*. Deaville, France.

Angevine C. L., Turcotte D. L., and Furnish M. D. (1982) Pressure solution lithification as a mechanism for the stick-slip behavior of faults. *Tectonics* **1**, 151-160.

Bathurst R. C. G. (1958) Diagenetic fabrics in some British Dinantian limestones. *Liv. and Manch. Geol. J.* **2**, 11-36.

Bayly B. (1985) Deformation with simultaneous chemical change: The thermodynamic basis. In *Metamorphic Reactions Kinetics, Textures, and Deformation* (eds. A. B. Thompson and D. C. Rubie). Advances in Physical Geochemistry 4, Springer Verlag, New York. pp. 269-277.

Bayly B. (1987) Nonhydrostatic thermodynamics in deforming rocks. *Can. J. Earth Sci.* **24**, 572-579.

Békri S., Thovert J. F., and Adler P. M. (1995) Dissolution of porous media. *Chem. Eng. Sci.* **50**, 2765-2791.

Békri S., Thovert J.-F., and Adler P. M. (1997) Dissolution and deposition in fractures. *Eng. Geol.* **48**, 283-308.

Botter B. J. (1985) Pore collapse measurements on chalk cores. *2nd North Sea Chalk Symposium*. Deauville, France.

Brignoli M., Papamichos E., and Santarelli F. J. (1995) Capillary effects in sedimentary rocks: application to reservoir water-flooding. *35th U.S. Symposium on Rock Mechanics*. Lake Tahoe, California.

Busenberg E. and Plummer L. N. (1986) A comparative study of the dissolution and crystal growth kinetics of calcite and aragonite. In *Studies in Diagenesis* (ed. F. A. Mumpton). U.S.G.S. Bulletin 1578, U.S. Geological Survey. pp. 139-168.

Carrio-Schaffhauser E. and Gaviglio P. (1990) Pressure solution and cementation stimulated by faulting in limestones. *J. Struct. Geol.* **12**, 987-994.

Chen W.-P. and Molnar P. (1983) Focal depths of intracontinental and intraplate earthquakes and their implications for the thermal and mechanical properties of the lithosphere. *J. Geophys. Res.* **88, B5**, 4183-4214.

Cox S. F. and Patterson M. S. (1991) Experimental dissolution-precipitation creep in quartz aggregates at high temperatures. *Geophys. Res. Letters* **18**, 1401-1404.

Da Silva F., Monjoie A., Debande G., Schroeder C., Poot B., Detiege C., and Halleux L. (1985) Mechanical behaviour of chalks. *2nd North Sea Chalk Symposium*. Stavanger, Norway, **2**, 1-10.

de Boer R. B. (1977) Pressure solution: Theory and experiments. *Tectonophysics* **39**, 287-301.

de Boer R. B., Nagtegaal P. J. C., and Duyvis E. M. (1977) Pressure solution experiments on quartz sands. *Geochim. Cosmochim. Acta* **41**, 257-264.

Delage P., Cui Y. J., and Schroeder C. (1996) Subsidence and capillary effects in chalks. *Eurock '96, ISRM International Symposium*. Torino, Italy, 1291-1298.

de Meer S. and Spiers C. J. (1995) Creep of wet gypsum aggregates under hydrostatic loading conditions. *Tectonophysics* **245**, 171-183.

de Meer S. and Spiers C. J. (1997) Uniaxial compaction creep of wet gypsum aggregates. *J. Geophys. Res.* **102, no. B1**, 875-891.

den Brok S. W. J. (1996) The effect of crystallographic orientation on pressure solution in quartzite. *J. Struct. Geol.* **18**, 859-860.

den Brok S. W. J. (1998) Effect of microcracking on pressure-solution strain rate: The Gratz grain-boundary model. *Geology* **26**, 915-918.

den Brok S. W. J. and Spiers C. J. (1991) Experimental evidence for water weakening of quartzite by microcracking and solution creep. *Geol. Soc. J.* **148**, 541-548.

Denbigh K. G. and Turner J. C. R. (1984) *Chemical Reactor Theory*. Cambridge University Press, Cambridge.

Dewers T. and Hajash A. (1995) Rate laws for water-assisted compaction and stress-induced water-rock interaction in sandstones. *J. Geophys.Res.* **100, no. B7**, 13093-13112.

Dewers T. and Ortoleva P. J. (1989) Mechano-chemical coupling in stressed rocks. *Geochim. Cosmochim. Acta* **53**, 1243-1258.

Dewers T. and Ortoleva P. (1990a) A coupled reaction/transport/mechanical model for intergranular pressure solution, stylolites, and differential compaction and cementation in clean sandstones. *Geochim. Cosmochim. Acta* **54**, 1609-1625.

Dewers T. and Ortoleva P. (1990b) Geochemical self-organization. III. A mechano-chemical model of metamorphic differentiation. *Am. J. Sci.* **290**, 473-521.

Dewers T. and Ortoleva P. (1991) Influences of clay minerals on sandstone cementation and pressure solution. *Geology* **19**, 1045-1048.

Elias B. P. and Hajash A. J. (1992) Changes in quartz solubility and porosity due to effective stress: An experimental investigation of pressure solution. *Geology* **20**, 451-454.

Elliot D. (1973) Diffusion flow law in metamorphic rocks. *Geol. Soc. Am. Bull.* **84**, 2645-2664.

Engelder T. (1982) A natural example of the simultaneous operation of free-face dissolution and pressure solution. *Geochim. Cosmochim. Acta* **46**, 69-74.

Evans B. and Kohlstedt D. L. (1995) Rheology of rocks. In *Rock Physics and Phase Relations* (ed. T. J. Ahrens). AGU Reference Shelf 3, American Geophysical Union, Washington, D.C. pp. 148-165.

Evans B., Bernabé Y., and Zhu W. (1999) Evolution of pore structure and permeability of rocks in laboratory experiments. In *Growth, Dissolution and Pattern Formation in Geosystems* (eds. B. Jamtveit and P. Meakin). Kluwer Academic Publishers, Dordrecht. pp. 327-344.

Gaviglio P., d'Albissin M. C., Bergerat F., and Vandycke S. (1993) Modifications de texture dans la craie au contact de failles normales: un exemple de graben dans le basin de Mons (Belgique). *Bull. Soc. géol. France* **164**, 565-575.

Gaviglio P., Adler P., Thovert J.-F., Vandycke S., Bergerat F., Békri S., and Lestideau R. (1997) Grain-scale microstructure and physical properties of faulted chalk. *Bull. Soc. géol. France* **168**, 727-739.

GBMR (1995) Craies et Schistes Krijt en Leisten Kreide und Schiefer Chalk and Shales. Colloquium Mundanum Proceedings, Brussels, Belgium.

Gibbs J. W. (1878) On the equilibrium of heterogeneous substances. Trans. Conn. Academy, III. In *The Scientific Papers of J. Willard Gibbs, Vol. 1*. Longman, Green, and Co., Toronto. pp. 343-524.

Gratier J.-P. (1993) Experimental pressure solution of halite by an indenter technique. *Geophys. Res. Letters* **20**, 1647-1650.

Gratier J.-P. and Gamond J. F. (1990) Transition between seismic and aseismic deformation in the upper crust. In *Deformation mechanisms, rheology and tectonics* (eds. R. J. Knipe and E. H. Rutter). Geological Society of London Special Publication 54, The Geological Society, London. pp. 461-473.

Gratier J.-P. and Guiguet R. (1986) Experimental pressure solution-deposition on quartz grains: the crucial effect of the nature of the fluid. *J. Struct. Geol.* **8**, 845-856.

Gratier J.-P., Chen T., and Hellmann R. (1994) Pressure solution as a mechanism for crack sealing around faults: Natural and experimental evidence. In *Proceedings of Workshop LXIII The Mechanical Involvement of Fluids in Faulting* (eds. S. Hickman, R. Sibson, and R. Bruhn). Open-file Report 94-228, U.S.G.S., Menlo Park. pp. 279-300.

Gratier J.-P., Renard F., and Labaume P. (1999) How pressure solution creep and fracturing processes interact in the upper crust to make it behave in both a brittle and viscous manner. *J. Struct. Geol.* **21**, 1189-1197.

Gratz A. J. (1991) Solution-transfer compaction of quartzites: Progress toward a rate law. *Geology* **19**, 901-904.

Hajash A. J. and Bloom M. (1991) Marine diagenesis of feldspathic sand: A flow-through experimental study at 200 °C, 1 kbar. *Chem. Geol.* **89**, 359-377.

Heidug W. K. (1995) Intergranular solid-fluid phase transformations under stress: The effect of surface forces. *J. Geophys. Res.* **100**, 5931-5940.

Heidug W. K. and Leroy Y. M. (1994) Geometrical evolution of stressed and curved solid-fluid phase boundaries 1. Transformation kinetics. *J. Geophys. Res.* **99**, 505-515.

Hellmann R. (1997) The albite-water system Part IV. Diffusion modeling of leached and hydrogen-enriched layers. *Geochim. Cosmochim. Acta* **61**, 1595-1611.

Hellmann R., Gratier J.-P., and Renders P. (1996) Deformation of chalk by pressure solution. *V.M. Goldschmidt Conference*. Heidelberg, Germany, **1**, 248.

Hellmann R., Gratier J.-P., and Chen T. (1998) Mineral-water interactions and stress: Pressure solution of halite aggregates. In *Water-Rock Interaction WRI-9* (eds. G. B. Arehart and J. R. Hulston). A.A. Balkema, Rotterdam. pp. 777-780.

Hickman S. and Evans B. (1995) Kinetics of pressure solution at halite-silica interfaces and intergranular films. *J. Geophys. Res.* **100**, 13113-13132.

Hickman S., Sibson R., and Bruhn R. (1995) Introduction to special section: Mechanical involvement of fluids in faulting. *J. Geophys. Res.* **100**, no. B7, 12831-12840.

Homand S., Shao J. F., and Schroeder C. (1998) Plastic modelling of compressible porous chalk and effect of water injection. *Eurock '98.* Trondheim, Norway, **2**, 495-504.

Hudson J. D. (1975) Carbon isotopes and limestone cement. *Geology* **3**, 19-22.

Jones M. E. and Leddra M. J. (1989) Compaction and flow characteristics of porous chalks. *Journée Craie*. Université de Lille, Lille, France.

Kamb W. B. (1959) Theory of preferred crystal orientation developed by crystallization under stress. *J. Geol.* **67**, 153-170.

Kamb W. B. (1961) The thermodynamic theory of nonhydrostatically stressed solids. *J. Geophys. Res.* **66**, 259-271.

Lasaga A. C. (1981) Rate laws of chemical reactions. In *Kinetics of Geochemical Processes* (eds. A. C. Lasaga and R. J. Kirkpatrick). Reviews in Mineralogy 8, Mineralogical Society of America, Washington, D.C. pp. 1-68.

Lehner F. K. (1990) Thermodynamics of rock deformation by pressure solution. In *Deformation Process in Minerals, Ceramics, and Rocks* (eds. D. J. Barber and P. G. Meredith). Unwin-Hyman, London. pp. 296-333.

Lehner F. K. (1995) A model for intergranular pressure solution in open systems. *Tectonophysics* **245**, 153-170.

Lehner F. K. and Bataille J. (1985) Nonequilibrium thermodynamics of pressure solution. *Pure Appl. Geophys.* **122**, 53-85.

Lemée C. and Guéguen Y. (1996) Modeling of porosity loss during compaction and cementation of sandstones. *Geology* **24**, 875-878.

Leroy Y. M. and Heidug W. K. (1994) Geometrical evolution of stressed and curved solid-fluid phase boundaries 2. Stability of cylindrical pores. *J. Geophys. Res.* **99**, 517-530.

Megnien C. (1980) Synthèse géologique du Bassin de Paris, *Mém. BRGM*, 101.

Merino E., Ortoleva P., and Strickholm P. (1983) Generation of evenly-spaced pressure-solution seams during (late) diagenesis: A kinetic theory. *Contrib. Mineral. Petrol.* **82**, 360-370.

Monjoie A., Schroeder C., Prignon P., Yernaux C., Silva F. D., and Debande G. (1990) Establishment of constitutive law of chalk and long term test. *3rd North Sea Chalk Symposium.* Copenhagen, Denmark, 1-17.

Monjoie A., Schroeder C., and Da Silva F. (1991) Testing procedure for time-dependent behaviour of chalk. *7th Intl. Congr. International Congress on Rock Mechanics*. Aachen, Germany, **7**, 565-567.

Mourzenko V. V., Békri S., Thovert J.-F., and Adler P. M. (1996) Deposition in fractures. *Chem. Eng. Communications* **148-150**, 431-464.

Mullis A. J. (1991) The role of silica preciptation kinetics in determining the rate of quartz pressure solution. *J. Geophys. Res.* **96**, 10007-10013.

Mullis A. M. (1993) Determination of the rate-limiting mechanism for quartz pressure solution. *Geochim. Cosmochim. Acta* **57**, 1499-1503.

Nakashima S. (1995) Diffusivity of ions in pore water as a quantitative basis for rock deformation rate estimates. *Tectonophys.* **245**, 185-203.

Ortoleva P., Chadam J., Merino E., and Sen A. (1987a) Geochemical self-organization II: The reactive-infiltration instability. *Am. J. Sci.* **287**, 1008-1040.

Ortoleva P., Merino E., Moore C., and Chadam J. (1987b) Geochemical self-organization I: Reaction-transport feedbacks and modeling approach. *Am. J. Sci.* **287**, 979-1007.

Paterson M. S. (1973) Nonhydrostatic thermodynamics and its geologic applications. *Rev. Geophys. Space Phys.* **11**, 355-389.

Paterson M. S. (1995) A theory for granular flow accomodated by material transfer via an intergranular fluid. *Tectonophys.* **245**, 135-151.

Pecqueur G., Mikolajczak A., and Siwak J. M. (1995) Etude expérimentale de deux craies en torsion. In *Craies et Schistes Krijt en Leisteen Kreide und Schiefer Chalk and Shales* (ed. GBMR). Colloquium Mundanum Proceedings, Brussels, Belgium. pp. 1.1.44-1.1.52.

Pharr G. M. and Ashby M. F. (1983) On creep enhanced by a liquid phase. *Acta Mettallica* **31**, 129-138.

Piau J. M. and Maury V. (1994) Mechanical effects of water injection in chalk reservoirs. *Proceedings Eurock '94* SPE/ISRM Intl. Conference. pp. 819-828.

Piau J. M. and Maury V. (1995) Basic mechanical modelisation of chalk/water interaction. In *Unsaturated Soils* (eds. Alonso and Delage). pp. 775-783

Plummer L. N. and Busenberg E. (1982) The solubilities of calcite, aragonite and vaterite in CO_2-H_2O solutions between 0 and 90 °C, and an evaluation of the aqueous model for the system $CaCO_3$ -CO_2 - H_2O. *Geochim. Cosmochim. Acta* **46**, 1011-1040.

Raj R. (1982) Creep in polycrystalline aggregates by matter transport through a liquid phase. *J. Geophys. Res.* **87 no. B6**, 4731-4739.

Raj R. and Chyung C. K. (1981) Solution-precipitation creep in glass ceramics. *Acta Metall.* **29**, 159-166.

Renard F. and Ortoleva P. (1997) Water films at grain-grain contacts: Debye-Hückel, osmotic model of stress, salinity, and mineralogy dependence. *Geochim. Cosmochim. Acta* **61**, 1963-1970.

Renard F., Park A., Ortoleva P., and Gratier J.-P. (1999) An integrated model for transitional pressure solution in sandstones. *Tectonophys.* **312**, 97-115.

Reuschlé T., Trotignon L., and Gueguen Y. (1988) Pore shape evolution by solution transfer: thermodynamics and mechanics. *Geophys. J.* **95**, 535-547.

Risnes R. and Flaageng O. (1999) Mechanical properties of chalk with emphasis on chalk-fluid interactions and micromechanical aspects. *Oil & Gas Science and Technology - Rev. IFP* **54**, 751-758.

Robin P.-Y. F. (1978) Pressure solution at grain-to-grain contacts. *Geochim. Cosmochim. Acta* **42**, 1383-1389.

Robin P.-Y. F. (1979) Theory of metamorphic segregation and related processes. *Geochim. Cosmochim. Acta* **43**, 1587-1600.

Rutter E. H. (1976) The kinetics of rock deformation by pressure solution. *Phil. Trans. R. Soc. Lond.* **A, 283**, 203-219.

Rutter E. H. (1983) Pressure solution in nature, theory and experiment. *J. Geol. Soc. London* **140**, 725-740

Rutter E. H. and Mainprice D. H. (1979) On the possibility of slow fault slip controlled by diffusive mass transfer processes. *Gerlands Beitr. Geophys.* **88**, 154-162.

Sallès J., Thovert J. F., and Adler P. M. (1993) Deposition in porous media and clogging. *Chem. Eng. Sci.* **48**, 2839-2858.

Schneider F., Potdevin J. L., Wolf S., and Faille I. (1996) Mechanical and chemical compaction model for sedimentary basin simulators. *Tectonophys.* **263**, 307-317.

Schroeder C. (1995) Le "pore collapse": Aspect particulier de l'interaction fluide-squelette dans les craies? In *Craies et Schistes Krijt en Leisteen Kreide und Schiefer Chalk and Shales*. (ed. GBMR). Colloquium Mundanum Proceedings, Brussels, Belgium. pp. 1.1.53-1.1.60.

Schroeder C., Bois A.-P., Maury V., and Hallé G. (1998) Water/chalk (or collapsible soil) interaction: Part II. Results of tests in laboratory on Lixhe chalk to calibrate water/chalk models. *Eurock '98*. Trondheim, Norway, **2**, 505-514 (SPE 47587).

Schroeder C. and Shao J. (1996) Plastic deformation and capillary effects in chalks. *5th North Sea Chalk Symposium*. Reims, France, 1-14.

Schutjens P. M. T. M. (1991) Experimental compaction of quartz sand at low effective stress and temperature conditions. *J. Geol. Soc. London* **148**, 527-539.

Schutjens P. M. T. M. and Spiers C. J. (1999) Intergranular pressure solution in NaCl: Grain-to-grain contact experiments under the optical microscope. *Oil & Gas Science and Technology - Rev. IFP* **54**, 729-750.

Shao J. F., Bederiat M., and Schroeder C. (1994) Elasto-viscoplastic modelling of a porous chalk. *Mechanics Res. Comm.* **21**, 63-75.

Sleep N. H. and Blanpied M. L. (1992) Creep, compaction and the weak rheology of major faults. *Nature 359*, 687-692.

Sorby H. C. (1863) On the direct correlation of mechanical and chemical forces. *Proc. Roy. Soc.* **12**, 538.

Spiers C. J. and Brzesowsky R. H. (1993) Densification behaviour of wet granular salt: Theory versus experiment. In *Seventh Symposium on Salt*, 1. Elsevier Science Publishers, Amsterdam. pp.82-92.

Spiers C. J. and Schutjens P. M. T. M. (1990) Densification of crystalline aggregates by fluid-phase diffusional creep. In *Deformation Processes in Minerals, Ceramics and Rocks* (eds. D. J. Barber and P. G. Meredith). Unwin Hyman, London. Chap. 12.

Spiers C. J., Schutjens P. M. T. M., Brzesowsky R., Peach C. J., Liezenberg J. L., and Zwart H. J. (1990) Experimental determination of constitutive parameters governing creep of rocksalt by pressure solution. In *Deformation Mechanisms, Rheology and Tectonics* (eds. R. J. Knipe and E. H. Rutter). Geological Society Special Publication No. 54, The Geological Society, London. pp. 215-227.

Tada R. and Siever R. (1986) Experimental knife-edge pressure solution of halite. *Geochim. Cosmochim. Acta* **50**, 29-36.

Tada R. and Siever R. (1989) Pressure solution during diagenesis: A review. *Ann. Rev. Earth Planet. Sci.* **17**, 89-118.

Tada R., Maliva R., and Siever R. (1987) A new mechanism for pressure solution in porous quartzose sandstone. *Geochim. Cosmochim. Acta* **51**, 2295-2301.

Urai J. L., Spiers C. J., Zwart H. J., and Lister G. S. (1986) Water weakening effects in rock salt during long term creep. *Nature* **324**, 554-557.

Weyl P. K. (1959) Pressure solution and the force of crystallization - a phenomenological theory. *J. Geophys. Res.* **64**, 2001-2025.

Wong P. K. and Oldershaw A. (1981) Burial cementation in the Devonian, Kaybob reef complex, Alberta, Canada. *J. Sediment. Petrol.* **51**, 507-520.